

# *Outcrop analog for an oolitic carbonate ramp reservoir: A scale-dependent geologic modeling approach based on stratigraphic hierarchy*

**Frédéric Amour, Maria Mutti, Nicolas Christ, Adrian Immenhauser, Gregory S. Benson, Susan M. Agar, Sara Tomás, and Lahcen Kabiri**

## **ABSTRACT**

Considerable effort has been devoted to the development of simulation algorithms for facies modeling, whereas a discussion of how to combine those techniques has not existed. The integration of multiple geologic data into a three-dimensional model, which requires the combination of simulation techniques, is yet a current challenge for reservoir modeling. This article presents a thought process that guides the acquisition and modeling of geologic data at various scales. Our work is based on outcrop data collected from a Jurassic carbonate ramp located in the High Atlas mountain range of Morocco. The study window is 1 km (0.6 mi) wide and 100 m (328.1 ft) thick. We describe and model the spatial and hierarchical arrangement of carbonate bodies spanning from largest to smallest: (1) stacking pattern of high-frequency depositional sequences, (2) facies association, and (3) lithofacies. Five sequence boundaries were modeled using differential global position system mapping and light detection and ranging data. The surface-based model shows a low-angle profile with modest paleotopographic relief at the inner-to-middle ramp transition. Facies associations were populated using truncated Gaussian simulation to preserve ordered trends between the inner, middle, and outer ramps. At the lithofacies scale, field observations and statistical analysis show a mosaiclike

## **AUTHORS**

FRÉDÉRIC AMOUR ~ *Institute of Earth and Environmental Science, Potsdam University, Karl-Liebknecht-Strasse 24-25, 14476 Potsdam-Golm, Germany; amour@geo.uni-potsdam.de*

Frédéric Amour completed his M.Sc. thesis (2007) on Triassic fluvial systems in western Europe at Rennes University, France. He is currently a Ph.D. candidate at Potsdam University, focusing on the investigation and modeling of two opposed platform morphologies—a Jurassic carbonate ramp in Morocco and an isolated platform in Italy. His main research interests include carbonate sedimentology, sequence stratigraphy, and outcrop modeling.

MARIA MUTTI ~ *Institute of Earth and Environmental Science, Potsdam University, Karl-Liebknecht-Strasse 24-25, 14476 Potsdam-Golm, Germany; mmutti@geo.uni-potsdam.de*

Maria Mutti holds degrees from the universities of Bologna, Wisconsin-Madison, and Milan. Following research at Eidgenössische Technische Hochschule Zürich and Woods Hole Oceanographic Institution, she has held faculty positions at the universities of Southern California and Stuttgart. In 2002, she joined the University of Potsdam as full professor of sedimentary geology. Her research focuses on carbonate systems and the integration of outcrop and subsurface studies.

NICOLAS CHRIST ~ *Faculty of Earth Sciences, Ruhr University, Universitätsstrasse 150, D-44801 Bochum, Germany; Nicolas.Christ@ruhr-uni-bochum.de*

Nicolas Christ is a postdoctoral researcher, whose interests are mainly focused on carbonate sedimentology, geochemistry, and diagenesis. He received his B.Sc. and M.Sc. degrees from the University of Strasbourg, France, and his Ph.D. from the University of Bochum, Germany. Nicolas is currently working as a researcher at the University of Bochum.

ADRIAN IMMENHAUSER ~ *Faculty of Earth Sciences, Ruhr University, Universitätsstrasse 150, D-44801 Bochum, Germany; adrian.immenhauser@rub.de*

Adrian Immenhauser presently holds the Chair for Sediment and Isotope Geology at Ruhr University. His main research interests include

Copyright ©2013. The American Association of Petroleum Geologists. All rights reserved.

Manuscript received March 6, 2012; provisional acceptance July 11, 2012; revised manuscript received September 25, 2012; final acceptance October 23, 2012.

DOI:10.1306/10231212039

carbonate sedimentology, diagenesis, and inorganic geochemistry. He received his diploma and Ph.D. from Bern University, Switzerland. Adrian has been the president of the Stratigraphy, Sedimentology, and Paleontology Division of European Geosciences Union, organized the International Association of Sedimentologists and Society for Sedimentary Geology-Central European Section conferences, and is the associate editor of several journals.

GREGORY S. BENSON ~ *ExxonMobil Upstream Research Company, P.O. Box 2189 URC-SW 639, Houston, Texas 77252; Gregory.S.Benson@ExxonMobil.com*

Greg Benson is a senior research geologist at ExxonMobil Upstream Research Company in Houston, Texas. He received his B.Sc. degree from the University of Southern California (1979) and his M.Sc. degree from the University of Arizona (1981). His interests include geomodelling, field studies, outcrop studies, internal consulting, mentoring, and teaching. Currently, Benson investigates new approaches to the geocellular modeling of fluvial systems.

SUSAN M. AGAR ~ *ExxonMobil Upstream Research Company, P.O. Box 2189 URC-SW 639, Houston, Texas 77272; susan.m.agar@exxonmobil.com*

Susan Agar is the director of the ExxonMobil (FC)<sup>2</sup> Alliance at the ExxonMobil Upstream Research Company, Houston, and is an honorary professor at Heriot-Watt University, Scotland. During her career in academia and industry, she has published on microstructural processes, deformation and fluid flow in accretionary prisms, rift tectonics, mid-ocean ridges and ophiolites, and flow in fractured reservoirs. She holds a Ph.D from Imperial College, London, and an M.A. degree in business administration from the Wharton School, University of Pennsylvania. Agar maintains a strong interest in promoting innovation through industry-academic interactions.

SARA TOMÁS ~ *Institute of Earth and Environmental Science, Potsdam University, Universitätsstrasse 150, D-44801, Potsdam-Golm, Germany; stomas@geo.uni-potsdam.de*

Sara Tomás received geology degrees from the University of Zaragoza (M.Sc.) and the University of Barcelona (Ph.D.), Spain. She is currently working at the University of Potsdam (Germany)

distribution that was simulated using a fully stochastic approach with sequential indicator simulation.

This study observes that the use of one single simulation technique is unlikely to correctly model the natural patterns and variability of carbonate rocks. The selection and implementation of different techniques customized for each level of the stratigraphic hierarchy will provide the essential computing flexibility to model carbonate settings. This study demonstrates that a scale-dependent modeling approach should be a common procedure when building subsurface and outcrop models.

## INTRODUCTION

The investigation of outcrop analogs is a key research tool for the improvement of carbonate reservoir characterization and modeling of subsurface hydrocarbon fields. Outcrop studies provide insights into the distribution and morphology of geologic bodies across a broad range of scales from tens of kilometers down to micrometer-scale features (Kerans et al., 1994; Kjensvik et al., 1994; Eaton, 2006; Mikes and Geel, 2006; Jones et al., 2008, 2009). One of the current challenges is the integration of various scales of geologic data and concepts into a single three-dimensional (3-D) model (Jones et al., 2009).

Within carbonate systems, facies associations across carbonate platforms and ramps (1–10 km [0.6–6.2 mi]) display gradational and ordered trends between neighboring depositional domains. In contrast, the spatial arrangement of lithofacies (1–100 m [3.3–330 ft]) shows a mosaiclike distribution pattern lacking clear and regular trends in facies-to-facies transitions (Wright and Burgess, 2005). A lithofacies mosaic appears to result from somewhat random processes during the deposition and preservation of carbonate sediments (Burgess, 2008). Each level of the stratigraphic hierarchy displays different distribution patterns, which requires a specific modeling technique designed to reproduce its unique characteristics (Falivene et al., 2006). Accordingly, the modeling of carbonate outcrop should involve the combination of various techniques to accommodate the scale-dependent nature of geologic heterogeneity.

Most of the previous modeling studies applied one single simulation method to model carbonate rocks. These methods span from surface-based modeling (Adams et al., 2005; Sech et al., 2009; Verwer et al., 2009) to interactive facies modeling (Willis and White, 2000; Aigner et al., 2007; Palermo

et al., 2010) and to algorithm-based modeling approaches (Kjonsvik et al., 1994; Aigner et al., 2007; Kenter et al., 2008; Tomás et al., 2010). Only a few studies—Zappa et al. (2006) on alluvial deposits and Koehrer et al. (2010) on dolomite bodies—tried to implement multiple simulation methods during facies modeling. We will demonstrate in this article that the building of a realistic 3-D geologic model must systematically combine various simulation techniques into the same modeling workflow to capture and model scale-dependent carbonate heterogeneities.

Previous outcrop modeling studies focused on carbonate systems have provided information about the morphology and dimension of shoals (Aigner et al., 2007; Qi et al., 2007; Palermo et al., 2010). These studies encompass areal dimensions on the order of 1 to 10 km (0.6–6.2 mi) in length and as much as 100 m (328.1 ft) in thickness. Shoal body dimensions can range significantly from 37 km (22.9 mi) in length and 4.2 m (13.7 ft) in thickness (Palermo et al., 2010) down to 1 km (0.6 mi) in length and 9 m (29.5 ft) in thickness (Qi et al., 2007). Other outcrop studies, such as those shown by Borkhataria et al. (2005) for a carbonate ramp and by Barnaby and Ward (2007) for a carbonate shelf, cover smaller areal dimensions (<1.5 km [0.9 mi] in length). Shoal complexes display lower lateral continuity ranging from 200 m (656.2 ft) to 1.3 km (0.8 mi) in length. Modern analogs also show similar variability of shoal morphology and dimensions (Harris, 2010). Significantly, all of these studies suggest that the large range of dimensional scatter depends on the scale of observation. The scale-dependent approach applied in this study has the advantage to simultaneously capture and model the large range of shoal complexity.

The aim of this study is the investigation and modeling of scale-dependent heterogeneities ranging from the stacking patterns of depositional sequences to the facies associations down to the individual lithofacies. Accordingly, this study documents a workflow designed to extract, for each of these spatial scales, geostatistical data on geobody morphology, dimensions, and association. We apply this approach to a 1-km (0.6-mi)–long and 100-m (328.1-ft)–thick well-exposed study window within a Jurassic oolitic carbonate ramp in the High Atlas mountain range of Morocco. Previous studies in this area (Pierre et al., 2010; Amour et al., 2012; Christ et al., 2012) provide the necessary basis for an in-depth analysis of the shoal complex. Our work has the potential to provide new insights on modeling capabilities that are of general use to improve simulation strategy of shallow-water carbonate systems.

as a lecturer and a research scientist on carbonate sedimentology. Her research focuses on sedimentary processes and environmental factors governing shallow-water and reefal carbonates of ancient systems in the Tethyan realm (Sardinia, Morocco, Oman).

LAHCEN KABIRI ~ *Faculty of Science and Technology, Moulay Ismail University, BP509 52000 Boutalmine, Errachidia, Morocco; Kabiri\_lahcen@yahoo.fr*

Lahcen Kabiri is a professor of geology at Moulay Ismail University and the coordinator and contributor of several national and international scientific events and projects. He has provided expertise to organizations such as Japan International Cooperation Agency, United Nations Development Programme, and United Nations Environment Programme. Lahcen is also the author and coauthor of several scientific publications including a book and oral presentations on the geology of the area of Errachidia.

## ACKNOWLEDGEMENTS

This project was financially supported by the ExxonMobil (FC)<sup>2</sup> Alliance, an ExxonMobil academic collaboration that focuses on the fundamental controls on flow in carbonates. We thank Martin Homann, Max Zitzmann, Fadi Semmo, Dennis Bunke, and Falko Kraul (University of Potsdam) for supporting us in the field. We also thank Gianluca Frijia and Matteo di Lucia (University of Potsdam) for their helpful comments. We thank Stephen N. Ehrenberg and Mark W. Longman for their constructive reviews. We also thank the “Ingenieurbüro” Gilan (Berlin) for the collection and processing of the LIDAR data and Simon Buckley (Centre for Integrated Petroleum Research, Bergen) for providing access to the LIDAR Interpretation and Manipulation Environment software. We thank Schlumberger for providing the three-dimensional geologic modeling software Petrel (Mark of Schlumberger). Finally, we thank all members of the Agouzil family for their hospitality in Amellago. The AAPG Editor thanks the following reviewers for their work on this paper: Stephen N. Ehrenberg and Mark W. Longman.

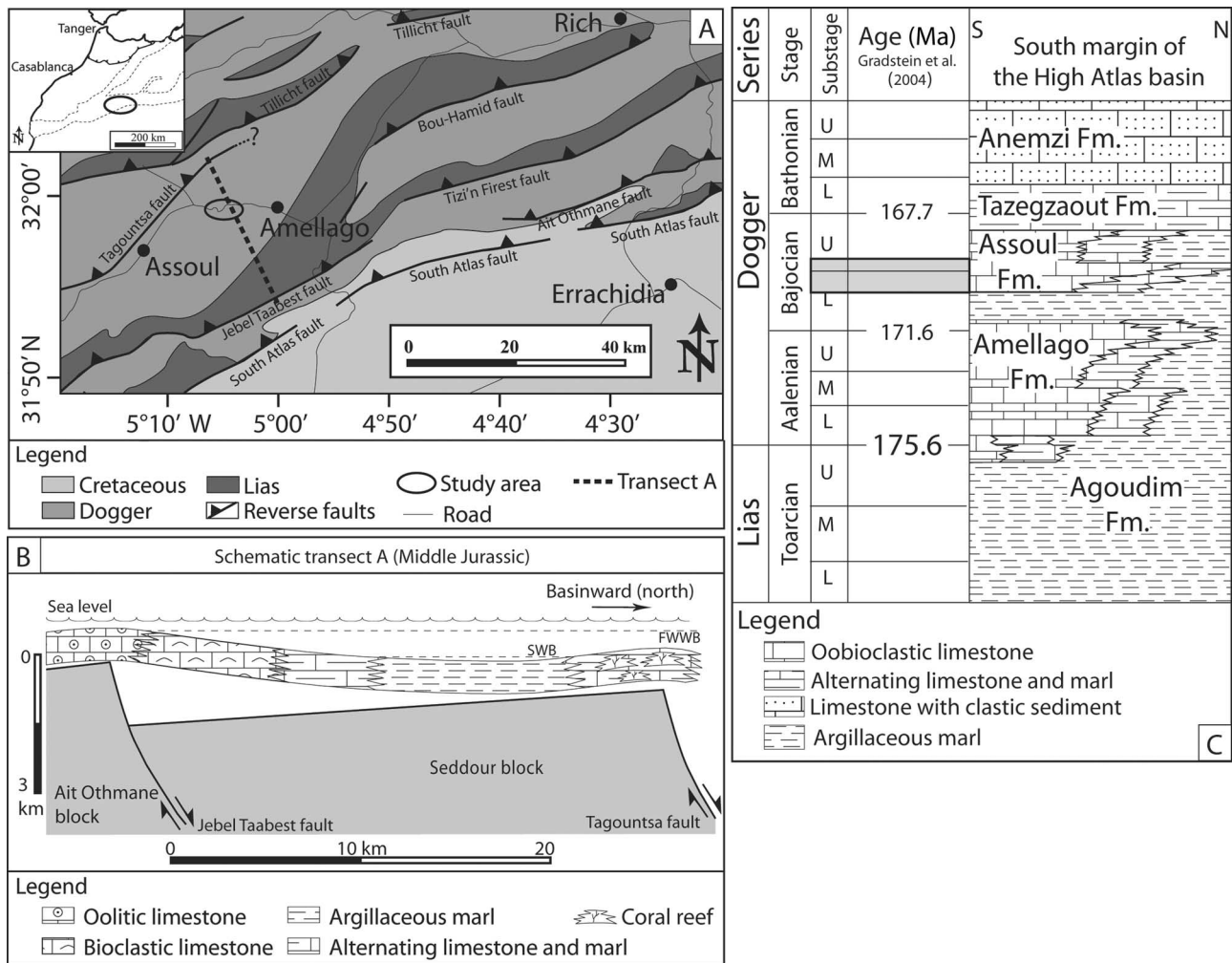


**Figure 1.** Geologic setting and location of the study area in the High Atlas mountain range (Morocco). (A) Geologic map of the southern margin of the central High Atlas mountain range (Wilmsen and Neuweiler, 2008; Pierre et al., 2010). (B) Schematic transect of the oolitic carbonate ramp during the Middle Jurassic (Poisson et al., 1998; Ait Addi, 2006). (C) Stratigraphic column of the Jurassic in the southern margin of the High Atlas basin (Pierre, 2006; Amour et al., 2012), with the study area shaded in gray. Fm = Formation; FWWB = fair weather wave base; SWB = storm-wave base.

### GEOLOGIC SETTING

The High Atlas mountain range of Morocco (Figure 1A) is a southwest-northeast orogen developed by the tectonic inversion of a Triassic–Jurassic rift system during the Cenozoic Alpine collision (Jacobshagen et al., 1988). The Triassic–Jurassic rift phase that initiated the aborted High Atlas rift basin (Manspeizer et al., 1978) is associated with the opening of the North Atlantic Ocean (Ziegler, 1994), leading to the breakup of Pangea. During the Early to Middle Jurassic, the High Atlas rift basin consisted of a seaway open to the northeast

connected to the Tethys (Bassoulet et al., 1993). Shallow-water carbonates were deposited within the platform margin, whereas the subsiding central part of the basin recorded rhythmic marls and limestones (Jacobshagen et al., 1988; Warme, 1988).

Within the southern margin of the central High Atlas rift basin, an early Toarcian crustal extension event (Laville et al., 2004) led to the dislocation of the carbonate platform into numerous rhomb-shape subbasins bounded by syndepositional ridges, which represented the crests of tilted blocks (Studer and du Dresnay, 1980; Poisson et al.,

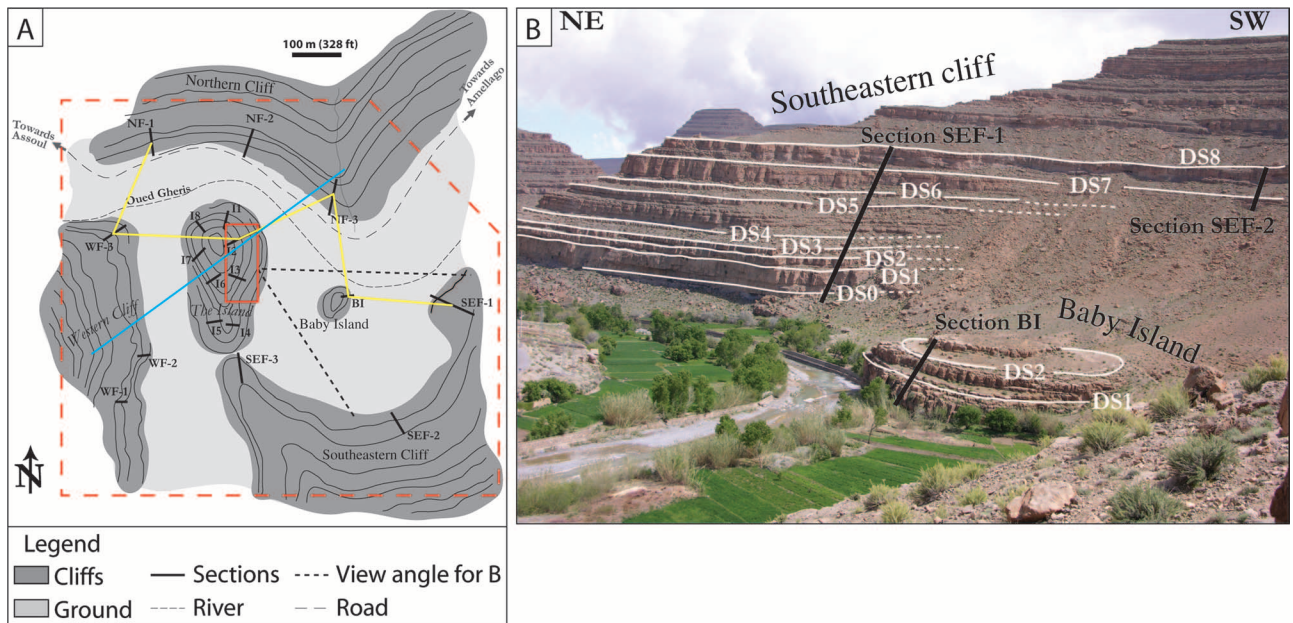


**Figure 2.** Overview of outcrop conditions within the study window. (A) Plan view of the outcrop with the location of described sections. The red box corresponds to Figure 8, and cross sections shown in Figure 4 (yellow) and in Figure 13 (blue) are located. The domain of modeling (dashed red) shown in Figures 10 and 12 is also displayed. (B) Pictures of the southeastern cliff and Baby Island outcrop. The view angle of the picture is shown in red on A. Five medium-scale (DS0, 3, 5, 7, and 8) and four small-scale sequence boundaries (DS1, 2, 4, and 6) were mapped. Three sections (black lines) are located in the photograph. DS = discontinuity surface.

1998) (Figure 1B). These topographic highs were characterized by shallow-water carbonate with episodic emersions, whereas hemipelagic marls were deposited within the troughs of subbasins (Stanley, 1981; Poisson et al., 1998). During the Aalenian to the Bajocian, carbonate platforms nucleated on the margins of the rhomb-shape subbasins (Ait Addi, 1998).

The study area is located in one of these subbasins, bounded by two synsedimentary faults: the Tagountsa fault to the north and the Jebel Taabest fault to the south (Figure 1A, B). In this subbasin, the Aalenian to Bajocian stratigraphic succession records two basinward progradation phases of a low-angle oolitic carbonate ramp from southwest to northeast, controlled by a second-order sea level fluctuation (Pierre et al., 2010). The two progradation phases were recorded by the Amellago Formation (Aalenian to lower Bajocian) (Poisson et al., 1998; Durllet et al., 2001; Pierre et al., 2010) and the Assoul Formation (middle? to upper Bajocian) (Amour et al., 2012; Christ et al., 2012). During the Bathonian and the Callovian, decreasing subsidence rate (Ellouz et al., 2003) favored the in-

filling of the central High Atlas rift basin by deltaic and continental deposits from the Anemzi Formation (Figure 1C).

The 220-m (721.8-ft)-thick Assoul Formation consists of an oolitic carbonate ramp (Amour et al., 2012; Christ et al., 2012) that displays stacking patterns and facies associations similar to the Amellago Formation (Durllet et al., 2001; Pierre et al., 2010). The Assoul Formation has been divided into three intervals: a lower grainy interval, a middle muddy interval, and an upper grainy interval (Christ et al., 2012). Grainy intervals represent the inner ramp with abundant oolitic and peloidal shoals. Alternating marls and limestones from the distal middle ramp characterize the middle muddy interval. The basal and top parts of the Assoul Formation record two progradation phases of the oolitic carbonate ramp (lower and upper grainy interval) toward the northeastern subbasin. Controlling factors on the evolution of the oolitic carbonate ramp of the Assoul Formation, such as sea level fluctuation, tectonic, climate, continental weathering, and runoff, are still under debate (Pierre et al., 2010; Christ et al., 2012).

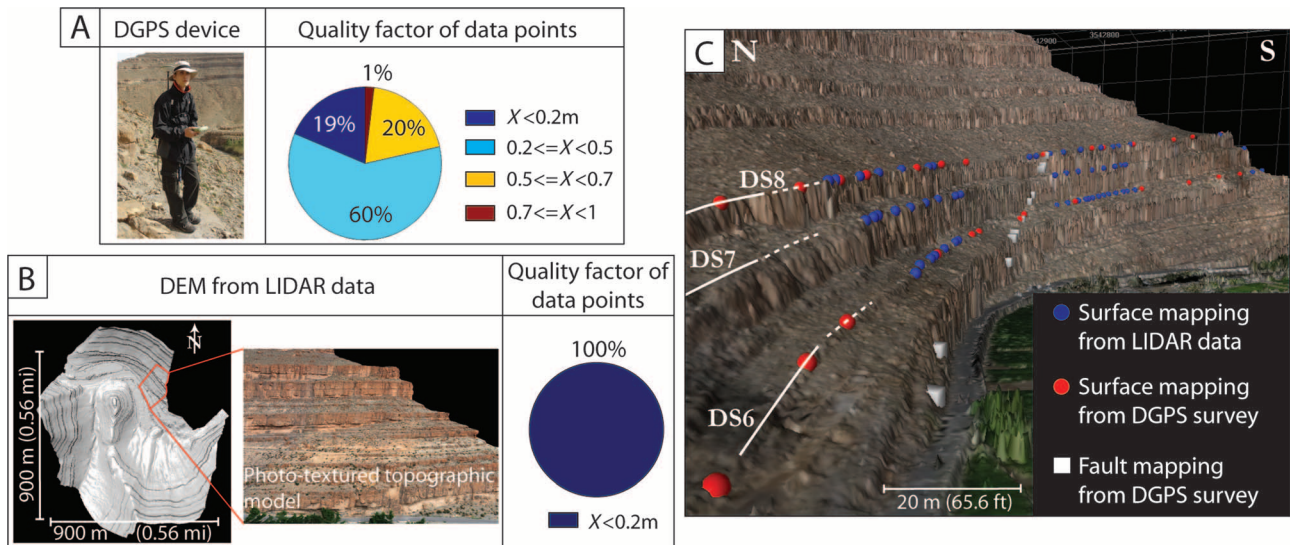


**Figure 3.** Comparisons between both georeferencing methods—differential global positioning system (DGPS) survey (A) and light detection and ranging (LIDAR) data (B)—applied to map key stratigraphic surfaces, sections, and faults. (A) DGPS mapping device in the field and pie chart, which compiles the quality factors of each data points. (B) LIDAR data set used to obtain a high-resolution digital elevation model (DEM) with a 0.2-m (0.7-ft) quality factor. Note the similar quality factor of DGPS points (a few tens of centimeters) between both mapping methods. (C) DEM gridded from LIDAR data demonstrating good fit between both LIDAR and DGPS georeferencing methods. DS = discontinuity surface.

## CHARACTERIZATION OF THE STUDY AREA

The study window (Figures 1, 2) is located within a 100-m (328-ft)-thick lower grainy interval of the Assoul Formation (Figure 1C). This interval corresponds to the first progradational pulse of the oolitic ramp system. During the Bajocian, the inner ramp is composed of kilometer-long oolitic and peloidal shoals with marly backshoal deposits. The foreshoal deposit is composed of intraclastic rudstones. The proximal middle ramp is composed of wackestone to packstone lithofacies including bioclasts of gastropods, corals, bivalves, cyanobacteria, and brachiopods. Toward the distal middle ramp, alternating limestone and marl facies is deposited and associated with molluscan-coral bioconstructions (Amour et al., 2012). The inner, middle, and outer ramp terminology is determined by the position of the fair weather wave base and storm-wave base (Burchette and Wright, 1992; Immenhauser, 2009). The stacking pattern of the Assoul Formation consists of high-frequency depositional sequences bounded by hardground surfaces. Isotopic measurements and catholuminescence analysis conducted on sequence boundaries

(Christ et al., 2012) reveal the absence of subaerial exposure features. These condensed surfaces are characterized by iron staining, borings, reworked mudclasts, and erosional depressions. The surfaces are interpreted to be related to maximum regression but nonemergent conditions (Christ et al., 2012).

## METHODS APPLIED AND TERMINOLOGY

### Field Methods

The well-exposed outcrop allowed the acquisition of 19 stratigraphic sections (Figure 2) with a section spacing ranging between 40 and 250 m (131–820 ft). Lateral tracing of beds and facies transitions were conducted between the sections. The aim was to investigate the dimensions and lateral variability of lithofacies and their associations. In the field, each section was logged, with an average of 3 to 4 samplings per meter to identify lithofacies. In addition, a total of 150 thin sections were analyzed in the laboratory to confirm the field-based lithofacies classifications. Paleocurrent features were measured in the field, and x-ray diffraction

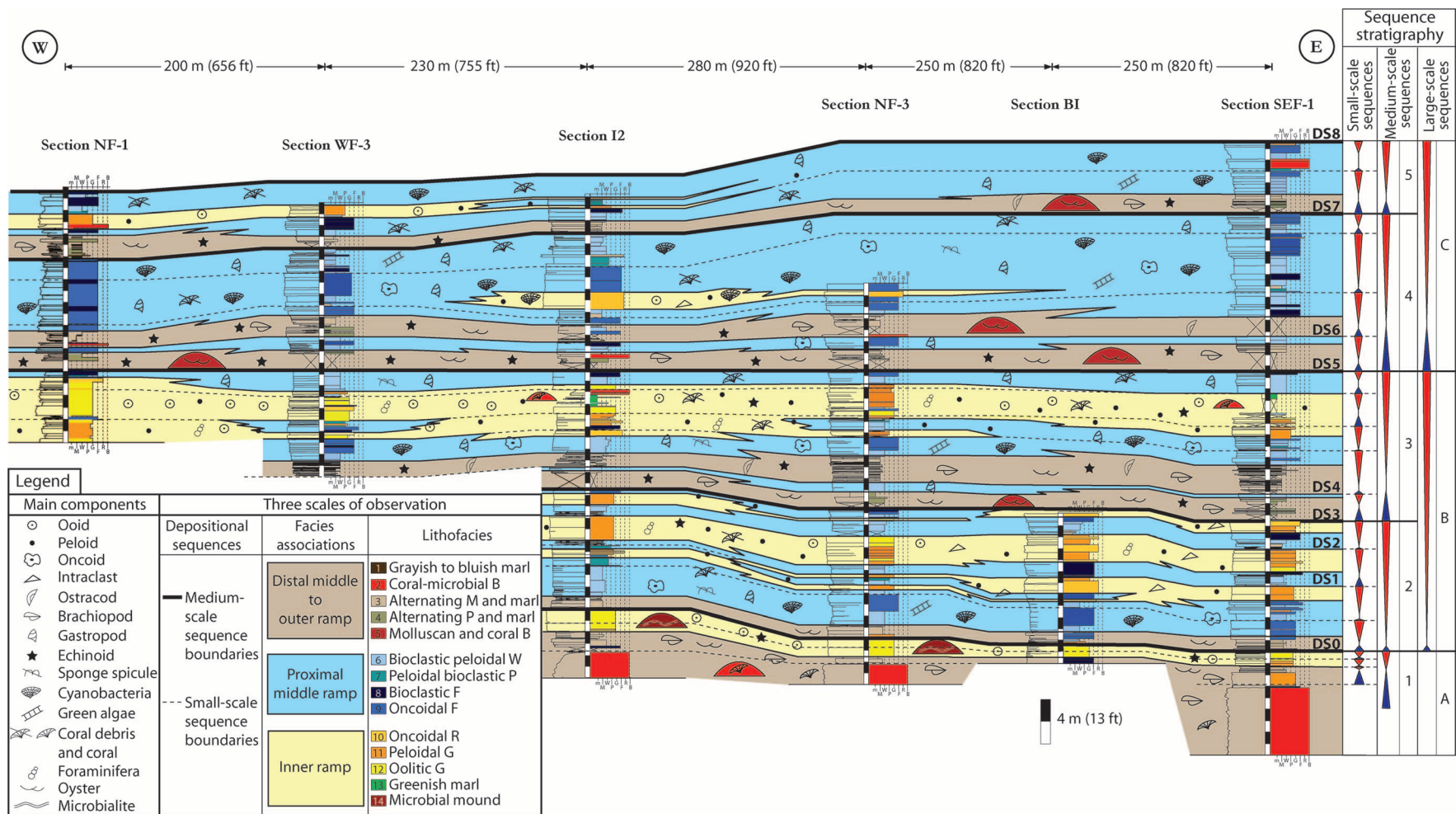


**Figure 4.** West-east cross section showing the facies distribution and sequence stratigraphy in the study area. Note the hierarchical relationship between the three scales of observation from depositional sequence to facies association and to lithofacies. Refer to Figure 2 for the location of the sections. DS = discontinuity surface; M = mudstone; W = wackestone; P = packstone; G = grainstone; F = floatstone; R = rudstone; B = boundstone.

**Table 1.** Lithofacies Classification and Interpretation

Lithofacies (Lf)		Lithofacies (Lf)	Texture**	Main Skeletal and Nonskeletal Components	Dimensions Used for Modeling	Main Sedimentary Features	Facies Associations
Nomenclature	Nomenclature*						
Lf 1		Grayish to bluish marl	m	Well-preserved brachiopods	Thickness: 12 m Length: 400 m Width: 400 m	15% of illite and quartz Horizontal laminations	Outer ramp
Lf 2		Coral-microbial-sponge reef	B	Scleractinian corals, microbialites, calcareous and siliceous sponges	Thickness: 12 m Length: 5–10 m Width: 5–10 m	Domal shape	Distal middle to outer ramp
Lf 3	2	Limestone beds with interbedded marl	m, M to W	Thin-shelled ostracods, echinoderms, and mollusks Subrounded micritic intraclasts in marl 15–20% of clastic sediments	Thickness: 2 m Length: 400 m Width: 400 m	Low to medium bioturbation Rhythmic input of clastic sediments Associated with meter-scale mollusk-dominated bioconstructions (Lf 5)	Distal middle ramp
Lf 4	3	Limestone beds with interbedded marl	m, W to P	Echinoderms, oysters, brachiopods, bryozoans, and coral debris Ferruginous peloids and subrounded micritic intraclasts	Thickness: 3.4 m Length: 400 m Width: 400 m	Low to medium bioturbation Rhythmic input of clastic sediments Associated with mollusk-dominated bioconstruction (Lf 5)	Distal middle ramp
Lf 5	10	Molluscan-coral-sponge reef	B	Oysters, brachiopods, bivalves, scleractinian corals, calcareous sponges, and demosponges Local deposition of marl	Thickness: as much as 6 m Length: 1–300 m Width: 1–230 m	Microencrustation by microbialites, bryozoans, and cyanobacteria Geopetal fabric	Distal middle ramp
Lf 6	4	Bioclastic peloidal limestones	W, W-P	Bivalves, cyanobacteria, gastropods, coral debris, green algae, and sponge spicules Rare echinoderms and agglutinated foraminifera Peloids and oncoids	Thickness: 2.6 m Length: 400 m Width: 400 m	Low to high bioturbation	Proximal middle ramp
Lf 7	5	Peloidal bioclastic limestones	W-P, P	Peloids with irregular shape Cyanobacteria, echinoderms, bryozoans, mollusks, and bivalves	Thickness: 1.3 m Length: 170 m Width: 130 m	Medium bioturbation	Proximal middle ramp

Lf 8	6	Bioclastic limestones	F	Centimeter-size gastropods, well-preserved coral debris, bivalves, brachiopods, and cyanobacteria Oncoids and peloids	Thickness: 0.8 m Length: 390 m Width: 360 m	Micritization Microencrustation by bryozoans, microbialite, and benthic foraminifera	Proximal middle ramp
Lf 9		Oncoidal limestones	F	Pluricentimetric oncoids and peloids Cyanobacteria, gastropods, well-preserved coral debris, and bivalves	Thickness: 1.8 m Length: 400 m Width: 370 m	Micritization Microencrustation by bryozoans, microbialites, cyanobacteria, and benthic foraminifera	Proximal middle ramp
Lf 10	9	Oncoidal limestones	R	Oncoids, peloids, ooids, and intraclasts Peloids and echinoderms as nucleus Cyanobacteria, gastropods, and mollusks	Thickness: 1 m Length: 210 m Width: 190 m	Brittle deformation Cement: crystal of sparite	Inner ramp
Lf 11	7	Peloidal limestones	G	Peloids and ooids Peloids and echinoderms as nucleus Echinoderms, agglutinated foraminifera, and gastropods	Thickness: 3.1 m Length: 260 m Width: 145 m	Cement: crystal of sparite No sedimentary structure	Inner ramp
Lf 12	8	Oolitic limestones	G	Ooids, composite ooids, and intraclasts Peloids and echinoderms as nucleus Bivalves, gastropods, and benthic foraminifera	Thickness: 2 m Length: 200 m Width: 140 m	Cross-bedding, bidirectional ripples and asymmetric ripples Bivalve encrustations on top of beds Sutured contact and brittle deformation Cement: crystal of sparite	Inner ramp
Lf 13	1	Grayish to greenish marl	m	Well-preserved brachiopods and bivalves Subrounded micritic intraclasts As much as 25% of clastic sediments	Thickness: 1 m Length: 170 m Width: 100 m	Interbedded with oolitic G (Lf 12)	Inner ramp
Lf 14		Microbial mound	B	Microbialites and sponges Ooids within growth cavities	Thickness: as much as 2 m Length: as much as 0.3–4 m Width: 0.3–4 m	Locally associated with oolitic G (Lf 12)	Inner ramp

\*Lithofacies type from Amour et al. (2012).

\*\*m = marl; M = mudstone; W = wackestone; P = packstone; G = grainstone; F = floatstone; R = rudstone; B = boundstone.

was used to determine the type and proportion of clay minerals in marly deposits.

## Statistical Analysis

In addition to field observations, the Kolmogorov-Smirnov (Press et al., 1992) test and semivariogram analysis (Gringarten and Deutsch, 2001) were performed to assess statistically the geologic heterogeneity.

The Kolmogorov-Smirnov test estimates the degree of fit between two data sets. In this study, the Kolmogorov-Smirnov test is used to compare a lithofacies thickness distribution based on sampled data against a theoretical thickness distribution characterized by an exponential growth equation. If the two distribution functions compare favorably, the outcrop-sampled thickness distribution can be assumed to exhibit an exponential growth. An exponential lithofacies distribution can indicate the occurrence of random (or stochastic) phenomena known as a Poisson process influencing the sedimentary record (Wilkinson et al., 1997, 1999; Burgess, 2008). A Poisson process implies that the thickness of a lithofacies type at one particular stratigraphic interval is independent of what has been previously preserved in the sedimentary record. A stratigraphic succession recording a Poisson process lacks trend on vertical changes in lithofacies thickness, leading to a random accumulation (or stochastic distribution) of lithologies. Conversely, the absence of a Poisson process implies a predictable component (or deterministic distribution) on the stacking pattern of lithofacies thickness. The Kolmogorov-Smirnov test is therefore an independent statistical tool that can be used to document the degrees of complexity of geologic heterogeneity.

Semivariograms (Gringarten and Deutsch, 2001) approximate geobody dimensions with major and minor directions of elongation and includes the azimuth of preferred orientation of the features. The minor direction semivariogram is calculated at a right angle to the major orientation. Variogram behavior such as hole effect (Gringarten and Deutsch, 2001) can provide further informa-

tion on geobody morphology. The hole effect, characterized by a variogram that oscillates periodically, indicates (sub)parallel, regularly spaced geobodies (en-echelon arrangement) over a large distance.

## Three-Dimensional Outcrop Modeling

A georeferencing survey of geologic data was performed using differential global position system (DGPS) mapping and light detection and ranging (LIDAR) scanning (Figure 3). For a more detailed description of the DGPS mapping method, please refer to Amour et al. (2012). Light detection and ranging data were used to (1) obtain an accurate digital elevation model and (2) map geologic features in inaccessible outcrop areas by picking surfaces and faults on the phototextured topographic model. The LIDAR data were interpreted using LIDAR Interpretation and Manipulation Environment (LIME), a viewing and interpretation software developed by Simon Buckley (Centre for Integrated Petroleum Research, Bergen). Discrepancies between the two data sets (DGPS points and LIDAR) are not noticeable, thanks to location accuracies better than 0.5 m (1.6 ft) in both mapping techniques (Figure 3).

Each geologic feature observed in the stratigraphic succession studied (Figure 4) is described using field observations and statistical analysis to establish a suitable modeling strategy. Then, each simulation methodology is combined in a single scale-dependent 3-D outcrop model.

## LITHOFACIES CLASSIFICATION AND DEPOSITIONAL SETTING

Previous investigations in this field area (Amour et al., 2012; Christ et al., 2012) have identified ten lithofacies. We integrate previous data sets with new sedimentologic data collected here to cover a larger area and present an expanded lithofacies classification consisting of a total of 14 lithofacies (Table 1). They were grouped into three facies associations: (1) an outer to distal middle ramp with alternating limestone and marl deposits, (2) a

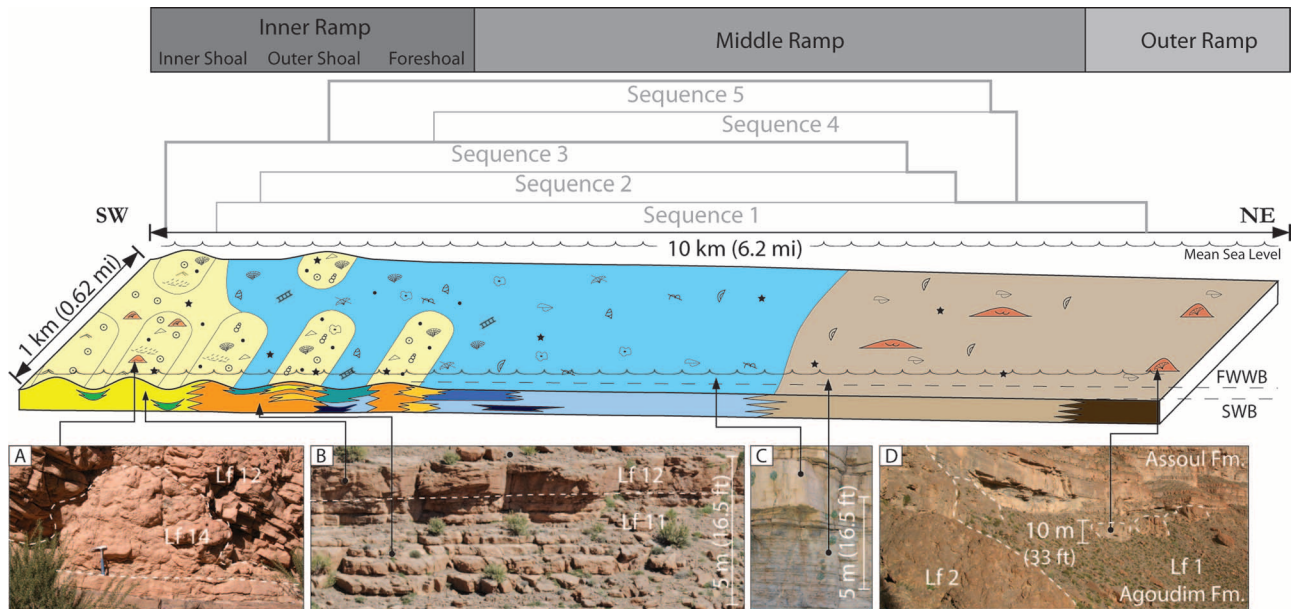


**Figure 5.** Paleodepositional reconstruction of the Bajocian carbonate ramp profile, with field pictures showing changes of lithofacies (Lf) types and bedding stacking pattern between depositional domains. Approximate medium-scale depositional sequence locations (gray line) showing the two main progradation phases (bold gray line) of the carbonate ramp in the study window. (A) Mud mound (Lf 14) surrounding by cross-bedded oolitic grainstone. Bedding contrasts within the inner ramp (B), proximal middle ramp, and distal middle to outer ramp (C). (D) Occurrence of coral-microbial bioconstructions (Lf 2) within the distal middle to outer ramp. Within the inner ramp, note the transition from inner ooid grainstone shoals (yellow) to outer peloid grainstone shoals (orange). Refer to Figure 4 for the Lf colors. Fm = Formation; FWWB = fair weather wave base; SWB = storm-wave base.

proximal middle ramp composed of wackestone to packstone lithofacies, and (3) an inner ramp dominated by grainstone lithofacies (Figure 4).

### Distal Middle to Outer Ramp

Five lithofacies types were recognized in this association. Grayish to bluish marls of lithofacies 1 are observed at the transition between the basal deposits of the Agoudim Formation and the initial shallow-water deposits of the basal Assoul Formation (Figure 5D). Bioclasts are rare and composed of well-preserved brachiopod shells. Horizontal laminations were also observed in the field. These two observations suggest a quiet open-marine environment below the storm-wave base and likely deposited in an outer ramp. Numerous coral-microbial bioherms (lithofacies 2) (Figure 5D) are present. These include platy to branching scleractinian corals, bryozoans, sponges, and microproblematic algae (*Thaumatoporella*). The intrareef deposits are mainly composed of microbialites, commonly

thrombolites (included with lithofacies 2). Alternating mudstone and marls and alternating packstone and marls (lithofacies 3 and 4) are also observed (Figure 5C). The biota of lithofacies 3 and 4 includes mainly bioclasts of echinoid spines, crinoids, bivalve, and ostracods. The lithology and the biota association for both lithofacies 3 and 4 indicate a low-energy, open-marine environment below the fair weather wave base and interpreted as a distal middle ramp. Molluscan-coral lithosomes (lithofacies 5) hundreds of meters long, mainly composed of oysters and brachiopods, developed in association with alternating ferruginous peloid packstone and marl deposits (lithofacies 4).

### Proximal Middle Ramp

This association of facies contains thick bioclastic peloidal wackestone beds (lithofacies 6) (Figure 5C) with micritized debris of bivalves, coral debris, gastropods, brachiopods, green algae, and textulariid foraminifera. Bioturbation is localized to pervasive,

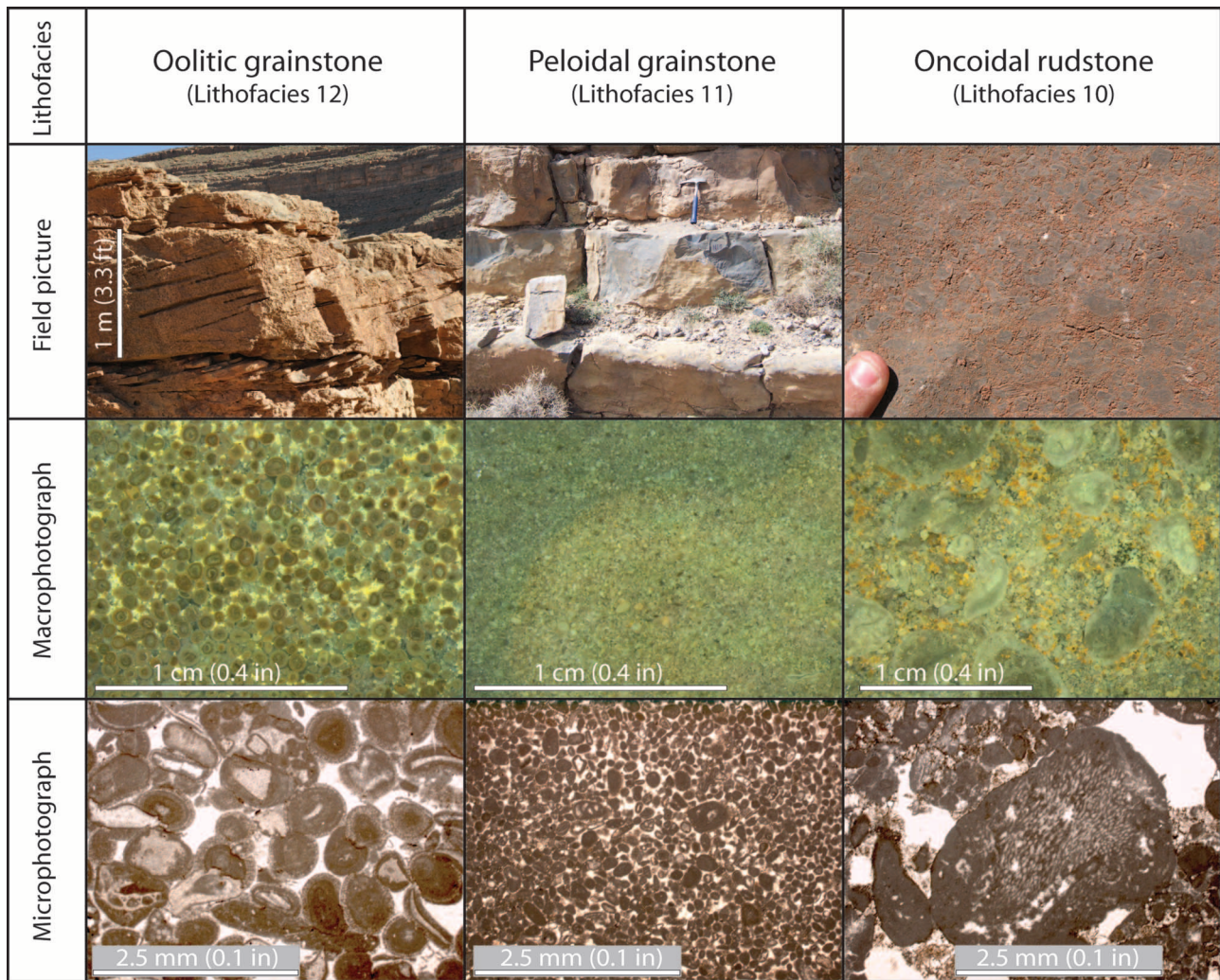


**Figure 6.** Micro- and macroscopic characterization of inner ramp lithofacies.

and abundant *Thalassinoides* burrows are recognized. Locally, peloids become dominant and represent as much as 60% of grains (lithofacies 7). Some ooids occur with increasing peloidal abundance, suggesting nearby shoal bodies. Oncoids forming floatstone bodies (lithofacies 9) as much as 4 m (13.1 ft) thick are abundant in the study window (Figure 4). The subrounded to rounded oncoids show filaments of cyanobacteria (*Cayeuxia*, *Rivularia*, and *Garwoodia*) in thin section. The occurrence of oncoids along with a relatively diverse biota and matrix-rich lithofacies association (Table 1) indicates an open-marine, shallow-water environment below the fair weather wave base and is interpreted as proximal middle ramp. Bioclastic floatstones (lithofacies 8) composed of

centimeter-size skeletal debris of gastropods, coral debris, bivalves, and brachiopods are observed at the top and base of depositional packages. Lithofacies 8 shows abundant micritization and microencrustation of bioclasts by bryozoans, microbialites, and cyanobacteria. Commonly associated with condensed surfaces, the bioclastic floatstone is interpreted to be the result of storm winnowing on the middle ramp during periods of low sedimentation rates.

### Inner Ramp

The inner ramp is composed of three grainstone lithofacies, plus grayish to greenish marls and occasional microbial mounds (Table 1). This lithofacies

association was subdivided into three subassociations, which record changes of depositional conditions across the inner ramp.

### Foreshoal

Rudstone bodies (lithofacies 10) composed of oncoids, which preserve filaments of cyanobacteria (*Cayeuxia*, *Rivularia*, and *Garwoodia*), were recognized in the field and thin section (right column of Figure 6). Peloids and ooids are abundant, and bioclasts of gastropods, textulariid foraminifera, unspecified mollusks, echinoderms, and large lituolinid foraminifera are present to common in abundance. The inorganic and organic components suggest the influence of both (1) the proximal middle ramp indicated by the occurrence of cyanobacteria and (2) the inner ramp characterized by the abundance of ooids. The texture of lithofacies 10 suggests a foreshoal located around the fair weather wave base. The foreshoal exhibits isolated, hundreds-of-meters-long, rudstone bodies with a thickness ranging from a few decimeters to 2 m (6.5 ft) (Figures 4, 5).

### Shoal Complex

The shoal complex is composed of peloidal grainstones (lithofacies 11) in the outer shoal and oolitic grainstones (lithofacies 12) deposited in the inner shoal (Figure 5B).

A few meters thick and a kilometer long, the outer shoal (Figure 4) consists of well-sorted peloidal grainstone (center column of Figure 6). Superficial ooids are present to common, but radial ooids are rare. The ooid nuclei are mainly peloids. No sedimentary structures have been recognized. The texture, sorting, and abundance of superficial ooids indicate moderate-energy conditions located above the fair weather wave base.

The inner shoal consists of shoals that are several meters thick, which can be traced laterally across the study area (Figure 4). The inner shoal is composed of superficial and radial ooids (left column of Figure 6) with lesser amounts of laminated fine-radial ooids. Their nuclei are peloids, echinoderms, and unspecified mollusk clasts. The dominance of superficial and radial ooids suggests moderate-energy conditions (Strasser, 1986). Sedi-

mentary structures such as cross-bedding, symmetric and asymmetric ripples, climbing ripples, and bidirectional ripples were measured in the field (Figure 7). The major paleoflow direction is 225°N. The record of symmetric and asymmetric ripples and cross-beddings indicates the presence of unidirectional and bidirectional currents, probably caused by tide and wave action. Microbial mounds (lithofacies 14) were observed at the base of the study window interbedded with oolitic grainstone (Figures 4, 5A). The fabric is microbial thrombolite with a few recrystallized platy and branching corals, calcareous sponges, and demosponges.

### Intershoal to Backshoal

Deposited between the oolitic shoal bodies are grayish to greenish marls (lithofacies 13) composed of 20 to 25% noncarbonate minerals, mostly illite and quartz. Oolitic grainstone bodies a few decimeters thick (lithofacies 12) were observed interbedded with the marls and show a medium- to poorly sorted fabric with micritic and oolitic intraclasts. The occurrence of oolitic grainstones interbedded with marls suggests an intershoal to backshoal with washover fan deposits from storms and high tides.

## DEPOSITIONAL SEQUENCES

The hierarchical stacking pattern displays cyclical changes of paleoenvironmental conditions (Figure 4). Because of the lack of biostratigraphic or radiometric data from the study area, this study chooses to apply a purely descriptive and time-independent nomenclature as defined by Strasser et al. (1999). Thus, the finest elementary sequences are called generically “small-scale” depositional sequences, and progressively larger medium- and large-scale depositional sequences are also recognized. The stratigraphic succession contains three large-scale sequences (A, B, and C) within which we identified five medium-scale sequences (1, 2, 3, 4, and 5). These sequences show a thickening trend toward the northeastern subbasin depocenter. Each sequence exhibits a thin deepening-upward trend at its base followed by a

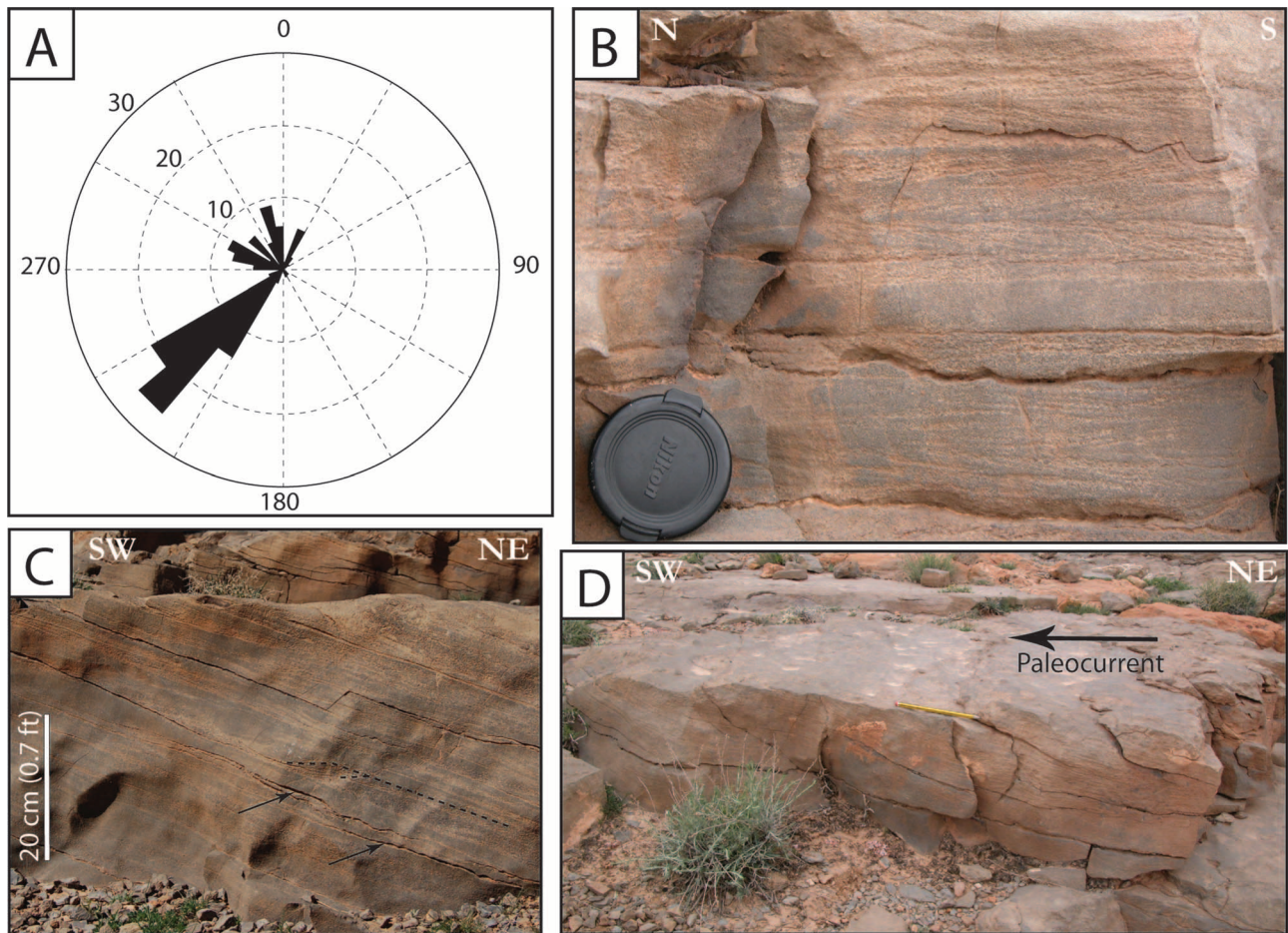


**Figure 7.** Paleocurrent features observed in oolitic grainstones. (A) Compilation of paleocurrent measurements showing a 225°N paleo-flow direction. (B) Bidirectional ripples suggesting alternating paleocurrent direction. (C) Internal structures of cross-beddings showing the presence of climbing ripples (dashed) and mud drapes (arrow). (D) Asymmetric ripples showing landward unidirectional current.

thick shallowing-upward trend marked at the top by a marine hardground.

Sequence boundaries are characterized by abrupt water depth changes from inner-ramp lithofacies below to distal middle-ramp lithofacies above. Both the medium- and large-scale sequences exhibit deepening-upward trends at their bases. At the base, the interval is characterized by an open-marine biota association composed of debris of echinoid spines, crinoids, bryozoans, and brachiopods from alternating bioclastic packstone and marl (lithofacies 4). The occurrence of terrigenous sediments (illite and quartz) within the interbedded marls, ferruginous peloids, and oyster-dominated lithosomes (lithofacies 5) suggests the contributions of continental hinterland. The clastic input is related

to the lowstand and early transgressive phase and reflects clastic sediment supply and basinward transport during low relative sea level. During the transgressive phase, a deepening-upward trend is interpreted from the progressive decrease of bioclast content upward and from the upward increase of alternating mudstone and marl (lithofacies 3). Evidence of a maximum flooding surface is lacking, so the maximum flooding timeline is approximated at the top of the thicker marl interval.

The expression of the shallowing-upward trend changes according to its position in the stratigraphic succession. The incomplete sequence A located at the top of the Agoudim Formation and at the base of the Assoul Formation reflects the onset of prograding shallow-water deposits into

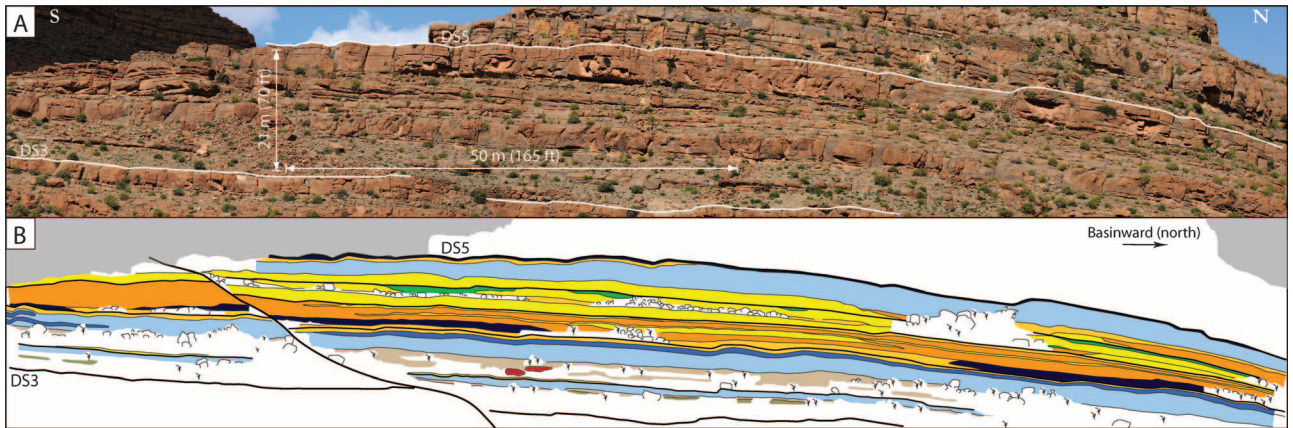


**Figure 8.** Transect of the east face of “Island” outcrop showing lithofacies distribution within the medium-scale sequence 3. (A) Field photograph displaying continuous and low-angle stratal pattern. (B) Two-dimensional lithofacies distribution observed in the field. Note the lateral and vertical lithofacies variability. At the larger scale of the facies association, a layer-cake stratal pattern is observed. Refer to Figure 4 for the lithofacies colors and Figure 2 for the location of the transect. DS = discontinuity surface.

the subbasin. The highstand deposits are characterized by the occurrence of microbial mounds interbedded with cross-bedded oolitic grainstone (Figure 5A). During the deposition of the large-scale sequence B, the highstand deposit is recorded by the occurrence of peloid-dominated shoals interbedded with foreshoal rudstone deposits within the medium-scale sequence 2. Next, the medium-scale sequence 3 records the occurrence of oolitic shoals associated with marly backshoal deposits. The latter lithofacies association suggests that sequence 3 records the maximum progradation of the carbonate ramp in the study window (Figure 5). In addition, the upper sequence boundary DS5 of medium-scale sequence 3 (Figure 4) is characterized by as much as five generations of *Gastrochaenolites*

borings. This feature is interpreted to record a long and complex omission history and provides evidence that DS5 is a major discontinuity surface. At the top of the stratigraphic interval, the incomplete large-scale sequence C records an increase of accommodation as shown by the dominance of wackestone to packstone lithofacies from the middle ramp and by the increase in thickness of small-scale depositional sequences. The medium-scale sequence 4 records the deposition of proximal middle-ramp deposits associated with isolated rudstone bodies. The medium-scale sequence 5 shows an increase of grainy lithofacies deposited in the outer and inner shoals, suggesting another prograding shoal phase recorded in the large-scale sequence C (Figure 5).

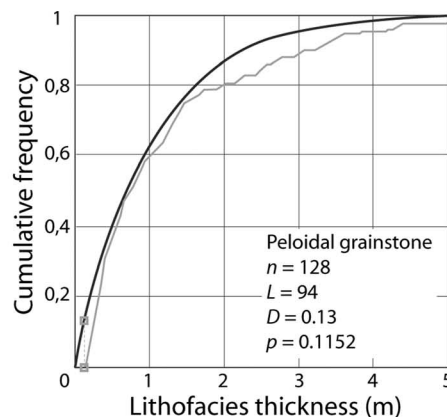
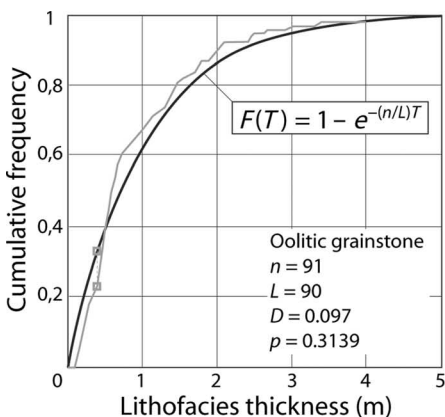


**Figure 9.** Theoretical exponential (black) and sampled (gray) cumulative frequency distribution of thicknesses of the oolitic grainstone (left) and the peloidal grainstone (right). The formula of the theoretical exponential distribution  $F(T)$  is outlined in black, where  $T$  is the thickness,  $n$  is the number of lithofacies units,  $L$  is the stratigraphic thickness studied, and  $p$  is the probability. The maximum difference between both curves is called “ $D$ ” (gray square).

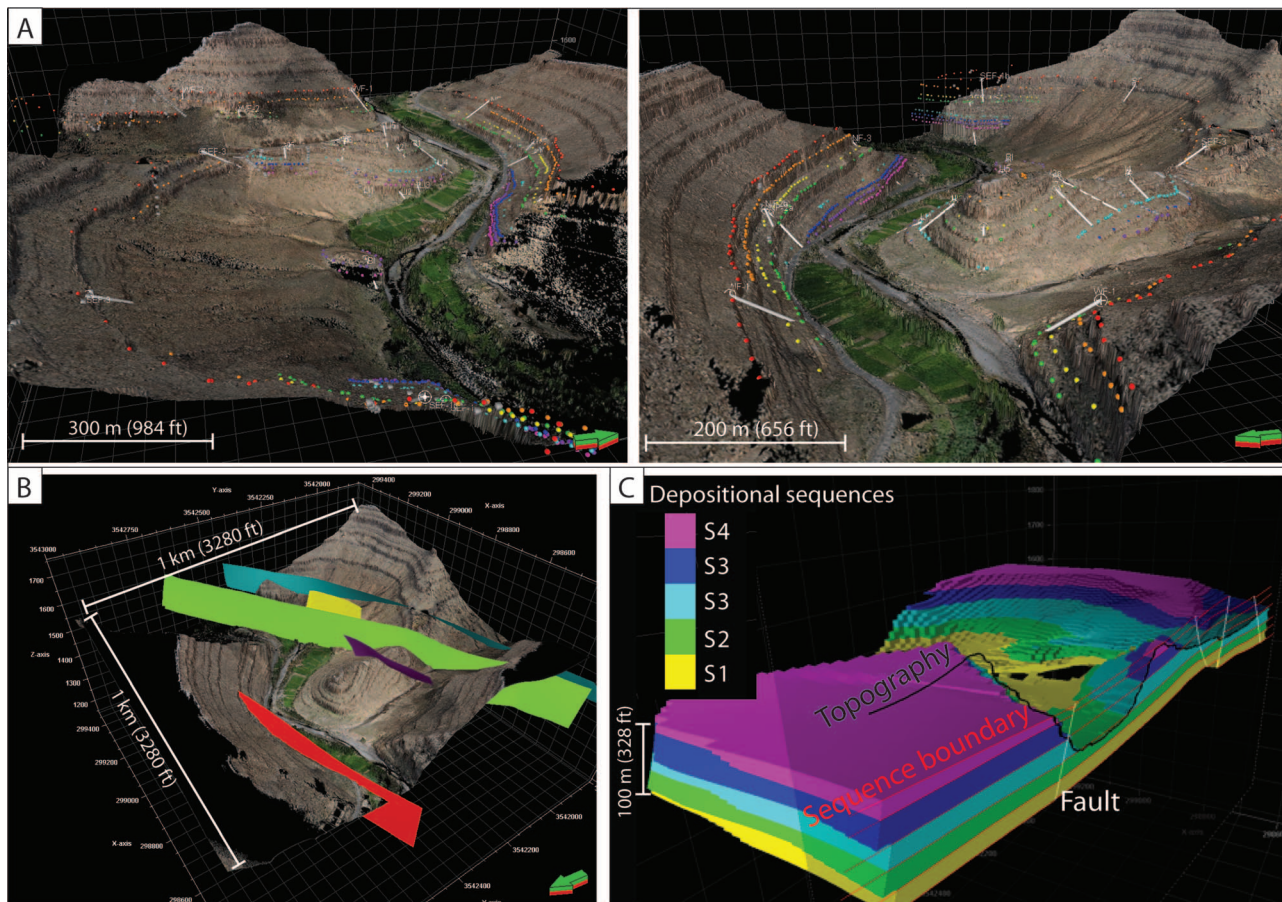


**Figure 10.** Input of geologic data and building of the model framework. (A) Two three-dimensional views of the input data, including the digital elevation model built from and light detection and ranging data and the field mapping differential global positioning system points of sequence boundaries (points) and faults (squares). Stratigraphic sections are located at the white lines in the images. (B) Dimensions of the digital outcrop model and location of the five major postdepositional faults modeled. (C) Construction of the depositional sequence model used as a framework for stochastic simulation. Refer to Figure 2 for the location of the three-dimensional pictures. S = depositional sequence.

## SCALE-DEPENDENT GEOLOGIC HETEROGENEITY

The choice of a suitable simulation methodology needs to be based on the intended scale of modeling, with considerations for the morphologies and spatial relationships between geologic bodies (Falivene et al., 2007). This study provides field observations and a statistical analysis of carbonate heterogeneity (Figures 8, 9) to (1) implement an adequate simulation methodology and then (2) justify our scale-dependent modeling strategy.

At the lithofacies scale, shoal bodies show a general shoaling-upward distal-to-proximal trend from oncoidal rudstone to peloidal grainstone to oolitic grainstone. This trend occurs in concert with

a change of bedding pattern from massive in the proximal to few-decimeters-thick beds in the distal (Figures 5B, 6). This conceptual approach of shoal distribution is acceptable at the basin scale but does not fully integrate field observations. For example, oncoidal rudstone not only shows vertical and lateral transition to oolitic and peloidal grainstone in the inner ramp, but also displays transitions with lithofacies deposited in the middle ramp (Figures 4, 8). The complexity of lithofacies distribution and association suggests a mosaiclike arrangement through the carbonate ramp, especially from the inner to proximal middle ramp.

The Kolmogorov-Smirnov statistical test was applied to lithofacies thickness distributions to assess statistically the geologic heterogeneity (Burgess,

2008). The test compares a sampled cumulative thickness distribution function with a theoretical exponential distribution function (Figure 9). The comparison estimates the difference,  $D$ , between both curves at each thickness. Then, a significance probability,  $p$ , is calculated to determine whether the maximum value of  $D$  occurs randomly in the present data set. If  $p$  is greater than 0.1, the candidate exponential distribution can be considered a good approximation to model the sampled lithofacies thickness curve. If  $p$  is less than 0.1, the exponential interpretation cannot be reasonably accepted. The test was conducted for oolitic grainstone ( $p = 0.3139$ ) and peloidal grainstone ( $p = 0.1152$ ) (Figure 9). Both lithofacies match the exponential function within tolerance, suggesting a stochastic distribution pattern at the lithofacies scale. The Kolmogorov-Smirnov test supports the interpretation of a mosaiclike arrangement as observed in the field.

The carbonate heterogeneity is less complex at the facies association scale than at the lithofacies scale. Despite the occurrence of interfingering at the transitions between facies associations (Figures 4, 8), the spatial relationships between the outer to distal middle ramp, proximal middle ramp, and inner ramp are known to be laterally ordered, indicating the existence of a deterministic component in their distribution. We conclude that geologic heterogeneity is more stochastically driven at the lithofacies scale than at the larger facies association scale. Consequently, the modeling methodology needs to consider the characteristics of each level of observation by adjusting the relative strengths of stochastic and deterministic methods during simulation.

## SCALE-DEPENDENT MODELING APPROACH

The methodology consists of three steps: (1) building the largest scale model based on the stacking patterns of medium-scale sequences (Figure 10), (2) modeling of facies association within the medium-scale sequences, and (3) the simulation of lithofacies distribution (Figures 11–13) within the facies association. Each step, which corresponds to

one level of the stratigraphic hierarchy, follows a specific modeling methodology adapted to its sedimentary features. Care was taken to capture the dimension and morphology of carbonate bodies during variogram analysis (Figure 11) and to properly model their distribution by comparing field-based (Figure 4) and stochastically simulated (Figure 13) geologic heterogeneity. The degree of concordance between input and output data was also used as a quality control factor. Within the geocellular model, the choice of cell dimensions is made by considering the size of the smallest geologic features that need to be simulated. Significant lithofacies such as peloidal grainstone and oncoidal floatstone are locally as thin as 0.2 m (0.7 ft) (Figure 4). Accordingly, the geocellular model was constructed with grid cells 0.1 m (0.3 ft) thick, considering that two cells are needed to adequately resolve a feature. A horizontal cell dimension finer than 15 m (49.2 ft) would have allowed the model to capture further lateral variations, but computing limitations dictated a larger cell dimension no less than 15 m (49.2 ft). Therefore, sedimentologic features below  $15 \times 15$  m ( $49.2 \times 49.2$  ft), such as coral-microbial-dominated bioherms (lithofacies 2) and microbial mounds (lithofacies 14), cannot be explicitly captured in the model. The model contains 909 conformable layers and 5.7 million cells.

## Modeling the High-Frequency Depositional Sequences

The first and largest scale of modeling is the construction of purely deterministic sequence-stratigraphic surfaces. Five medium-scale sequence boundaries (DS0, 3, 5, 7, and 8), four small-scale sequence boundaries (DS1, 2, 4, and 6), five post-depositional faults, and 19 stratigraphic sections (Figure 10) were input to the model as gridded elevation surfaces. A total of 5001 DGPS and LIDAR points were used to georeference these geologic data (Figure 3). Sequence boundary surfaces were created using the minimum curvature algorithm with a 10-m (32.8-ft) grid node spacing. The five zones built in the model correspond to the five medium-scale depositional sequences described

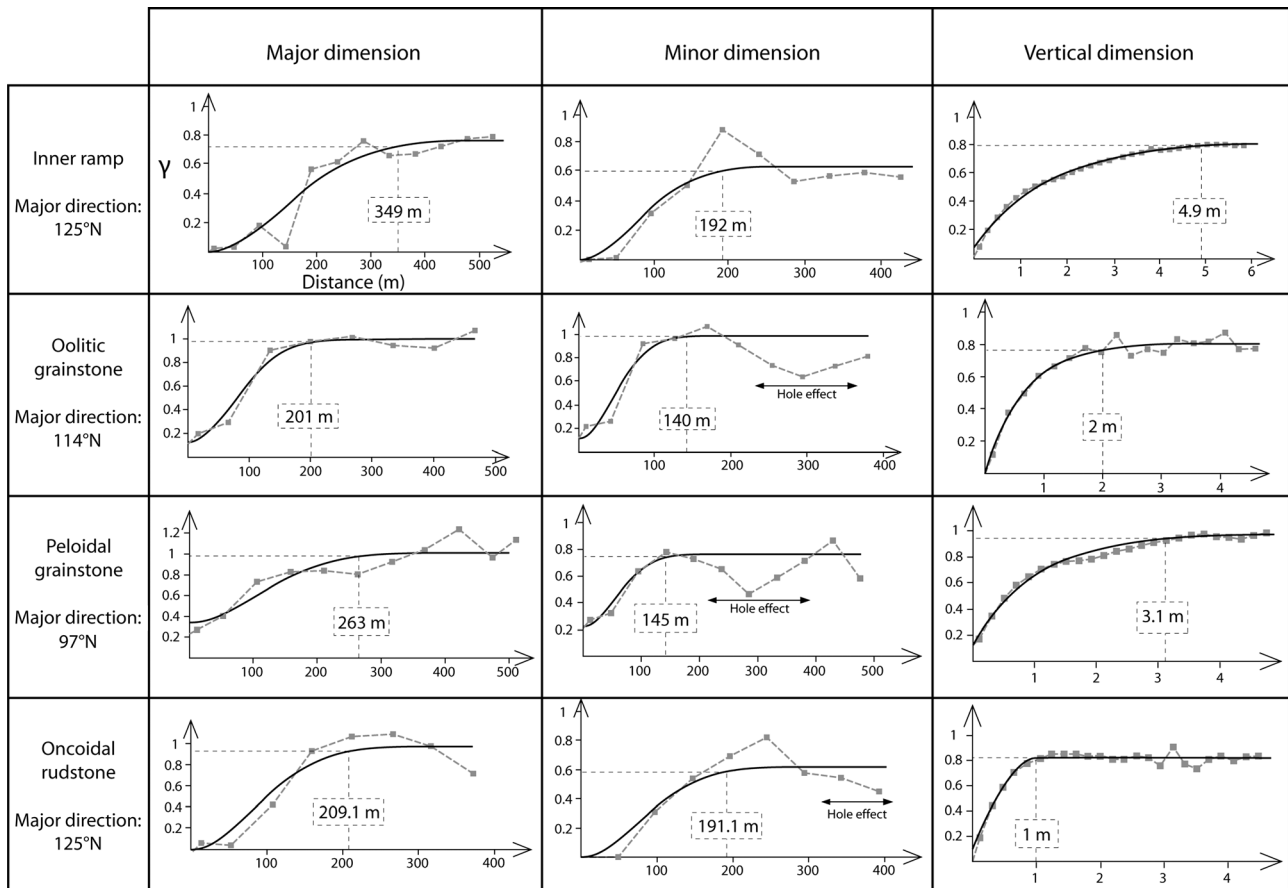


**Figure 11.** Summary of the major, minor, and vertical dimensions of inner-ramp shoals and inner-ramp lithofacies using semi-variograms, which are plots of the semivariance  $\gamma$  against the distance. Note the fitting of experimental variograms (dashed gray curve) with idealized type semivariograms (black curve). Oscillations in the experimental variograms (hole effect) indicate the regularly spaced periodicity of features. The hole effect observed in the minor variograms of oolitic grainstone, peloidal grainstone, and oncoidal rudstone suggests en-echelon arrangement of the geobodies.

above (Figures 4, 10C). Despite the high density of DGPS and LIDAR points, additional user-defined control points were necessary to extrapolate as realistically as possible sequence boundaries across valleys and to avoid edge effects. The additional control points were carefully created to be consistent with the sequence thicknesses and fault offsets measured in the field.

The mapping of medium-scale sequence boundaries reveals a general continuous and low-angle (0.03–0.25°) dipping depositional profile toward the northeast. The depositional profile becomes steeper toward the land and exhibits a 4-m (13.1-ft) paleotopographic relief at the transition between the outer and inner shoal complexes (Figure 13).

## Modeling the Facies Association

The second modeling step populates facies associations that characterize the inner, middle, and outer ramp within each medium-scale sequence. This step uses the stochastic algorithm truncated Gaussian simulation (TGSim) because it preserves the ordered transitions between the depositional domains of the ramp (Figure 5) while allowing the use of conditioning tools, such as probability trends, during stochastic simulation. Particular attention was focused on the semi-variogram analysis of the morphology of shoal bodies (see above), which is a key interpretive input to the TGSim algorithm. Vertical and horizontal semi-variograms are plots of the semivariance  $\gamma$  against the sample-pair

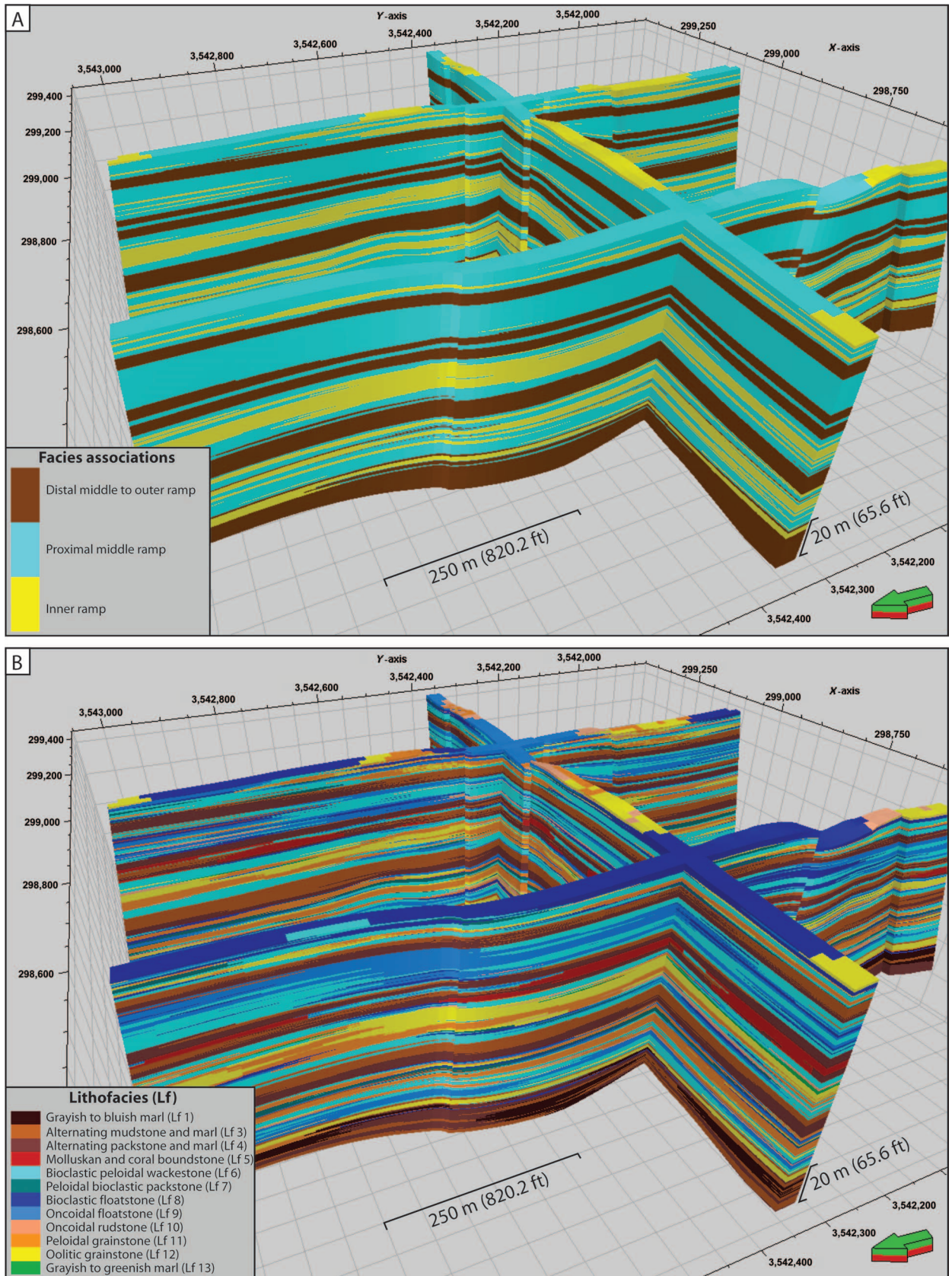


**Figure 12.** Three-dimensional view of the facies association model (A) and lithofacies model (B) (vertical exaggeration, 3×). Note the constraints of lithofacies occurrence and distribution within each facies association. Refer to Figure 2 for the location of the three-dimensional pictures.

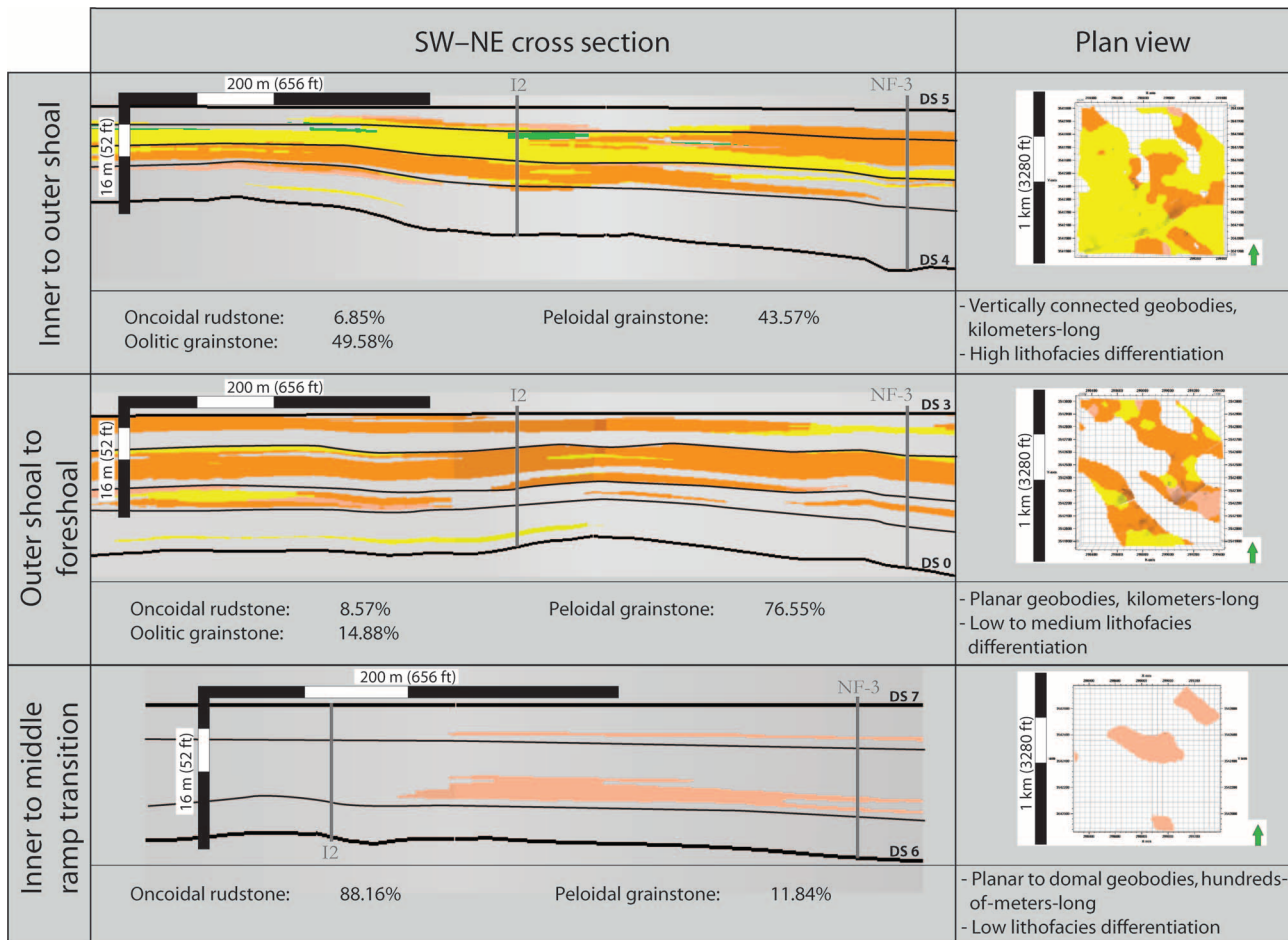


**Figure 13.** Southwest-northeast cross sections (left) of the scale-dependent model located within the inner ramp and representative model layer plan view maps (right). In the maps, note the strongly oriented and relatively well-connected distributions of the facies association tracts (all but the subject facies association are filtered out and appear in gray) and the comparatively patchy mosaic of lithofacies (yellow, orange, and tan). Note the topographic relief at the transition between inner and outer shoals. Refer to Figure 12 for the lithofacies colors and to Figure 2 for the location of the cross sections. DS = discontinuity surface.

separation distance called “lag” distance (Figure 11). To calculate the vertical semivariogram, a 0.1-m (0.3-ft) lag distance was chosen to match the resolution of described sections. The lag distance for the horizontal semivariogram was 50 m (164 ft), approximately the smallest between-section spacing.

The inner ramp represents 25% of the study area and contains interconnected, 350-m (1148.3-mi)-long, 190-m (623.3-ft)-wide, and 5-m (16.4-ft)-thick shoal bodies (Figure 11). The preferred orientation of elongation is 125°N, which is in agreement with paleocurrent measurements (Figure 7). Three different types of shoal morphology were recognized (Figures 12, 13) in field observations (Figure 4). The most distal shoals are found at the transition between the proximal middle ramp and the inner

ramp and consist of isolated, approximately 300-m (985-ft)-long and as much as 2-m (6.6-ft)-thick rudstones. The landward increase of horizontal and vertical connectivities between shoal bodies leads to more complex morphologies. The outer shoal to foreshoal are characterized by planar, kilometer-long, and as much as 4-m (13.1-ft)-thick shoals (Figures 4, 13). The stacking pattern of small-scale sequences displays a significant vertical compartmentalization of shoals separated by matrix-rich middle-ramp bodies. Therefore, the vertical shoal connectivity observed in the model (and in the field) is low. Toward the most proximal part of the ramp, the vertical connectivity across the small-scale sequence boundaries leads to more complex shoal body morphologies (Figure 13). The inner

shoal is planar to domal, kilometer long, and as much as 8 m (26.2 ft) thick.

### Modeling the Lithofacies

For the final step, the three depositional domains of the carbonate ramp (Figure 12A) are filled by their unique association of lithofacies (Figure 12B). This modeling step captures the degrees of geologic differentiation within the three types of shoal bodies (Figure 13). Both the mosaiclike lithofacies distribution (Figures 8, 9) and the morphological contrasts between lithofacies bodies (Figure 11) (Table 1) can be simulated using sequential indicator simulation (SISim). Sequential indicator simulation is used because (1) its method of populating lithofacies between data points can be independent of any geologic trend and does not enforce lateral associations and (2) a unique semi-variogram can be assigned to each lithofacies type. The operating mode of SISim is flexible enough to honor the observed variations in heterogeneity with one exception: the molluscan-coral bioherms (lithofacies 5) were modeled using object-based modeling to create a scattered population of domal bioconstructions.

Semivariogram analysis shows that each lithofacies is characterized by its own dimensions and preferred orientation. In the inner ramp, the hole effect (Gringarten and Deutsch, 2001; see above) is observed within the minor axis lithofacies semi-variograms (central column of Figure 11), indicating the occurrence of subparallel, regularly spaced lithofacies bodies with an average interbody spacing of approximately 349 m (1145 ft). Oolitic grainstones constitute 32.8% of the inner ramp and average 200 m (656.2 ft) in length, 140 m (459.3 ft) in width, and 2 m (6.6 ft) in thickness, with a spacing of approximately 300 m (985 ft). These bodies have a preferred elongation orientation of 114°N. Peloidal grainstones (56.9% of the inner ramp) are 260 m (853.0 ft) long, 145 m (475.7 ft) wide, and 3.1 m (10.2 ft) thick and are oriented 97°N, with a subparallel spacing of approximately 300 m (985 ft). The oncoidal rudstone (10.3% of the inner ramp) shows significant anisotropy in vertical and horizontal dimensions.

The 210-m (688.9-ft)-long, 190-m (623.3-ft)-wide, and 1-m (3.3-ft)-thick rudstone bodies exhibit a nearly isotropic morphology.

The three types of shoal bodies observed within the inner ramp display significant changes in their lithofacies associations (Figures 4, 13). Within the proximal middle ramp, isolated shoal bodies comprise mainly oncoidal rudstone and a lesser fraction of peloidal grainstone. Oolitic grainstone is absent. Within the outer shoal to foreshoal, we find kilometers-long planar shoal bodies composed of peloidal grainstones with common and locally deposited oolitic grainstones and oncoidal rudstones (Figure 13). In the most proximal part of the inner ramp, shoal bodies show a high degree of heterogeneity, characterized by vertical stacking and lateral transition between peloidal and oolitic grainstones (Figure 13). A low fraction of oncoidal rudstone occurs as thin and discontinuous layers.

## DISCUSSION

### Scale-Dependent Geologic Heterogeneity and Its Controlling Factors

Along the depositional profile of the Bajocian carbonate ramp of the Assoul Formation, a clear proximal-distal linear trend between facies associations (Figure 5) is evidenced by lateral lithofacies variability (Figures 4, 13) and the distribution of organic and inorganic components (Figure 6) (Table 1). The kilometer-long shoal complex of the inner ramp can be divided into three distinct shoal bodies with different morphologies from proximal to distal: (1) planar to domal, kilometer long, as much as 8 m (26.2 ft) thick; (2) planar, kilometer long, as much as 4 m (13.1 ft) thick; and (3) isolated, hundreds-of-meters-long shoals at the transition between the inner ramp and the proximal middle ramp (Figure 13). The Bajocian carbonate ramp displays two episodes of basinward progradation through the stratigraphic succession (Figures 4, 5), which are likely controlled by change of accommodation. This assumption is consistent with field observations that display a clear relationship between the type of lithofacies and the thickness

of depositional sequences (Figures 4, 5, 13). The abundance of grainstone lithofacies increases within thin depositional sequences, whereas wackestone to packstone lithofacies association dominates in thicker sequences. In addition, the vertical variability of both lithofacies type and thickness of depositional sequences shows repetitive deepening- and shallowing-upward trends, suggesting a relative sea level fluctuation and an associated change in accommodation as a major controlling factor on the studied stratigraphic succession. For comparison, the Amellago Formation underlying the Assoul Formation shows a similar oolitic ramp profile and a comparable stacking pattern of lithofacies and depositional sequences. A tens-of-kilometers-long study of the Amellago Formation (Pierre et al., 2010) also suggested that the oolitic carbonate ramp was primarily controlled by accommodation changes.

At the bedding scale, the lithofacies heterogeneity cannot be fully explained by accommodation changes. A lithofacies mosaic (Figures 8, 9) implies local changes of environmental conditions (clastic input, turbidity, hydrodynamic level, storm frequency, water geochemistry, or nutrient availability), which affect carbonate precipitation and transport at a similar water depth (Rankey, 2004; Wright and Burgess, 2005; Strasser and Védérine, 2009). In this study, the oolitic-dominated inner shoal and peloidal-dominated outer shoal consisted of a mosaic of grainstone lithofacies, marls, and microbial mounds (Figures 4, 13), suggesting that intrinsic parameters such as hydrodynamic level, storm events, tidal parameters, or differential fluvial input add to the inherent lithofacies disorder. The occurrence of both linear and mosaic arrangements of carbonate bodies within the Assoul Formation are mainly controlled by external and internal factors, respectively.

### **Scale-Dependent Geologic Modeling**

The study window displays scale-dependent geologic heterogeneity, where each stratigraphic level displays specific sedimentary features (Figure 14). This study establishes a different simulation method designed to reproduce the unique characteristics of each of those levels (Figure 14). The modeling

techniques extend from a deterministic approach at the largest stratigraphic architecture scale to an environment-specific stochastic approach at the smallest lithofacies scale (Figure 14). A purely stochastic algorithm like SISim, which was used to simulate mosaiclike lithofacies patterns, should not be used to model the entire study window. If we had chosen to apply only the SISim algorithm, the ordered transitions between the facies association across the depositional profile would not have been captured, and the final model would have included significant errors in terms of geobody placement and association. However, TGSim can only use a single variogram for all facies, which is clearly an oversimplification of the geologic reality (Figure 11), and its operating mode produces a poor approximation of the observed lithofacies mosaic (Amour et al., 2012). The above examples highlight the difficulty of modeling carbonate rocks by applying one single method. Each algorithm has unique capabilities and drawbacks (Journel et al., 1998; Falivene et al., 2006, 2007) that, in one location or another, would incorrectly render the field observations.

### **Geologic Heterogeneity and Modeling Strategy: Recommendations**

During the last two decades, advances in the field of statistical analysis and field-based observations of geologic heterogeneity within modern (Wilkinson and Drummond, 2004) and ancient shallow-water carbonate systems (Wilkinson et al., 1997, 1999; Burgess, 2008; Strasser and Védérine, 2009) have emphasized the common abundance of a mosaic-like distribution of lithofacies, the finest scale of our modeling strategy. At the coarser basin scale, the association of lithofacies, characterizing similar depositional conditions, tends to exhibit less spatial disorder in the sedimentary record. Facies associations display then a more gradational and linear arrangement between carbonate bodies along a proximal-distal depositional profile (Wright and Burgess, 2005), as shown here and in previous studies (Gischler and Lomando, 1999; Aurell and Bádenas, 2004; Bádenas and Aurell, 2010; Pierre et al., 2010).

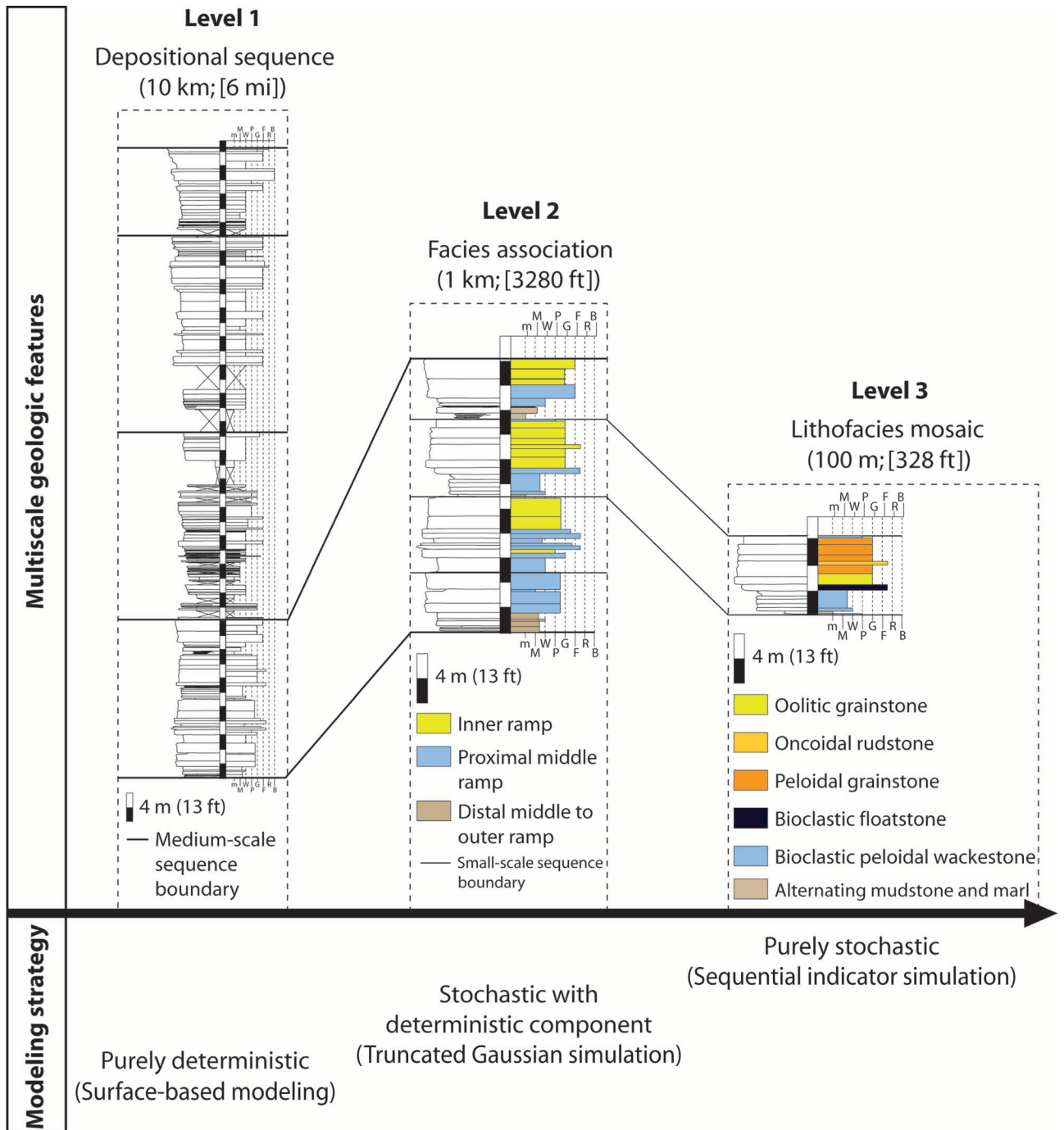


**Figure 14.** Summary of scale-dependent geologic features based on section SEF-1 from the large-scale stacking pattern of high-frequency depositional sequences (level 1) to the intermediate-scale facies association (level 2) and to the finest-scale lithofacies types (level 3). The modeling strategy that was used for each level is noted across the bottom. Note the alignment between the observed spatial arrangement of geologic features and the capabilities of simulation techniques chosen for each set of features. Refer to Figure 2 for the location of section SEF-1. M = mudstone; W = wackestone; P = packstone; G = grainstone; F = floatstone; R = rudstone; B = boundstone; m = marl.

During the same two decades, outcrop and subsurface modeling has known remarkable enhancements of the simulation tools used (Coburn et al., 2006). These improvements were resulted

from the large number of simulation techniques that were being constantly refined (Gringarten and Deutsch, 2001; Coburn et al., 2006; Kenter et al., 2008; Jones et al., 2009) and successfully

applied to model carbonate systems. These simulation techniques include a deterministic approach with surface-based modeling to capture the architecture of carbonate platforms (Sech et al., 2009) and an algorithm-based method to stochastically populate carbonate bodies (Aigner et al., 2007; Pöppelreiter et al., 2008; Tomás et al., 2010). Each method has been compared and contrasted in outcrop facies models to assess their major advantages and drawbacks (Falivene et al., 2006, 2007; Aigner et al., 2007; Amour et al., 2012). Considerable effort has been devoted to the generation and improvement of simulation tools and techniques, whereas a reflection on how to best combine them into a single 3-D model has been lacking (Zappa et al., 2006; Koehrer et al., 2010).

The inability for a single simulation method to correctly render all sedimentary features is illustrated by the need to resort to interactive facies correction (pixel painting to correct facies distribution) during simulations (Willis and White, 2000; Aigner et al., 2007; Palermo et al., 2010). A scale-dependent modeling approach takes advantage of the abilities of each technique, whereas its drawbacks can be offset by the use of other simulation tools and thus provide essential computing flexibility to model carbonate rocks. The selection of an appropriate combination of simulation tools involves a full knowledge of carbonate heterogeneity at each level of the stratigraphic hierarchy. In addition, the implementation of multiple techniques into the same workflow requires the development of innovative modeling methodologies. Better understanding of modern and ancient carbonate systems (e.g., Lehrmann and Goldhammer, 1999; Wilkinson et al., 1999; Wright and Burgess, 2005; Strasser and Védrine, 2009) should guide the design of simulation strategies. A scale-dependent modeling approach promises to be a valuable method to build outcrop and subsurface models.

## CONCLUSIONS

The investigation of a study area 1 km (3280.1 ft) wide and 100 m (328.1 ft) thick within a Bajocian oolitic carbonate ramp has demonstrated the need

for a scale-dependent modeling approach ranging from the large-scale stacking pattern of depositional sequences down to the facies associations at the intermediate scale and ultimately down to lithofacies types at the finest scale. An individual simulation method has been customized for each hierarchical level of heterogeneity based on the characteristics needed to be integrated into the 3-D outcrop model. Field observations and statistical analysis have documented the variability of shoal morphologies, dimensions, distributions, and associations and provides new perspectives on modeling strategies that take advantage of algorithm strengths and capabilities.

- Fourteen shallow-marine lithofacies were identified and grouped into three main facies associations: an inner ramp, a proximal middle ramp, and a distal middle to outer ramp. The inner ramp was further subdivided into sub-association, an intershoal to backshoal with marly deposits, an oolitic inner shoal, a peloidal outer shoal, and a foreshoal with oncoidal rudstones. The stratigraphic architecture shows five medium-scale sequences composed of four to five small-scale sequences.
- Scale-dependent geologic heterogeneity within the Assoul Formation requires the combination of both a deterministic and stochastic approach to realistically capture and model the spatial geobody arrangement. The largest scale model, comprising the structural and stratigraphic framework and stacking pattern of depositional sequences, was built using a deterministic surface-based modeling approach. The next scale model, the facies association, was modeled using TGSim to portray the ordered trends observed between facies associations. Finally, the finest scale features, individual lithofacies, were modeled using SISim because of its tendency to produce spatially independent lithofacies elements. Additionally, object-based modeling was used to insert discrete bioherm objects into the facies model.
- The first modeling step focused on sequence boundary morphologies. The depositional profile is a low-angle ( $0.03\text{--}0.25^\circ$ ) ramp with a

4-m (13.1-ft) topographic high at the transition between the inner and outer shoals. At the facies association scale, the kilometers-long shoal complex of the Assoul Formation is composed of (1) planar-to-domal, kilometer-long, and as much as 8-m (16.4-ft)-thick shoals in the proximal part of the inner ramp; (2) planar, kilometer-long, and 3- to 4-m (9.8–13.1-ft)-thick shoals within the outer shoal and foreshoal; and (3) isolated, hundreds-of-meters-long, and 1- to 2-m (3.3–6.6-ft)-thick foreshoal bodies at the transition between the proximal middle ramp and the inner ramp. At the finest scale of modeling, each grainstone lithofacies, characterized by its own unique dimensions, occurs in different proportions within the three types of shoal bodies. The linear and gradational trend between facies associations is influenced by changes in accommodation, whereas intrinsic parameters such as hydrodynamic level, storm events, and differential fluvial input controlled the lithofacies mosaic.

- The use of one single simulation technique across all scales is unlikely to produce a realistic 3-D model of shallow-water carbonate systems. The implementation of several techniques adapted to each level of the stratigraphic hierarchy will (1) provide essential computing flexibility for simulation and (2) lead to better integration of the geologic heterogeneity in a 3-D model. If further efforts are devoted to the methods to combine several simulation techniques into a modeling workflow, we will produce better geologic models and thus improve subsurface reservoir simulations at the interwell spacing.

## REFERENCES CITED

- Adams, E. W., J. P. Grotzinger, W. A. Watters, S. Schröder, D. S. McCormick, and H. A. Al-Siyabi, 2005, Digital characterization of thrombolite-stromatolite reef distribution in a carbonate ramp system (terminal Proterozoic, Nama Group, Namibia): *AAPG Bulletin*, v. 89, p. 1293–1318.
- Aigner, T., S. Braun, D. Palermo, and W. Blendinger, 2007, 3-D geological modeling of a carbonate shoal complex: Reservoir analog study using outcrop analogs: *First Break*, v. 25, p. 65–72.
- Ait Addi, A., 1998, New sedimentologic and geodynamic data on the Aalenian–Lower Bajocian facies of the High Atlas of Morocco (northern Errachidia): *Comptes Rendus de l'Académie des Sciences*, v. 326, p. 193–200.
- Ait Addi, A., 2006, The dogger reef horizons of the Moroccan central High Atlas: New data on their development: *Journal of African Earth Sciences*, v. 45, p. 162–172, doi:10.1016/j.jafrearsci.2006.01.011.
- Amour, F., M. Mutti, N. Christ, A. Immenhauser, S. M. Agar, G. S. Benson, S. Tomás, R. Always, and L. Kabiri, 2012, Capturing and modeling meter-scale spatial facies heterogeneity in a Jurassic ramp setting (central High Atlas, Morocco): *Sedimentology*, v. 59, p. 1158–1189, doi:10.1111/j.1365-3091.2011.01299.x.
- Aurell, M., and B. Bádenas, 2004, Facies and depositional sequence evolution controlled by high-frequency sea level changes in a shallow-water carbonate ramp (late Kimmeridgian, NE Spain): *Geological Magazine*, v. 141, p. 717–733, doi:10.1017/S0016756804009963.
- Bádenas, B., and M. Aurell, 2010, Facies models of a shallow-water carbonate ramp based on distribution of nonskeletal grains (Kimmeridgian, Spain): *Facies*, v. 56, p. 89–110, doi:10.1007/s10347-009-0199-z.
- Barnaby, R. J., and W. B. Ward, 2007, Outcrop analog for mixed siliciclastic-carbonate ramp reservoir: Stratigraphic hierarchy, facies architecture, and geologic heterogeneity: Grayburg Formation, Permian Basin, U.S.A.: *Journal of Sedimentary Research*, v. 77, p. 34–58, doi:10.2110/jsr.2007.007.
- Bassoulet, J. P., A. Poisson, S. Elmi, F. Cecca, Y. Bellion, R. Guiraud, Y. M. Le Nindre, and J. Manivit, 1993, Middle Toarcian paleoenvironments, *in* J. Dercourt, L. E. Ricou, and B. Vrielynck, eds., *Atlas Tethys paleoenvironmental maps*: Paris, France, Gauthier-Villars, p. 63–80.
- Borkhataria, R., T. Aigner, M. C. Pöppelreiter, and J. C. P. Pipping, 2005, Characterization of epeiric “layer-cake” carbonate reservoirs: Upper Muschelkalk (Middle Triassic), The Netherlands: *Journal of Petroleum Geology*, v. 28, p. 15–42, doi:10.1111/j.1747-5457.2005.tb00076.x.
- Burchette, T. P., and V. P. Wright, 1992, Carbonate ramp depositional systems: *Sedimentary Geology*, v. 79, p. 3–57, doi:10.1016/0037-0738(92)90003-A.
- Burgess, P. M., 2008, The nature of shallow-water carbonate lithofacies thickness distribution: *Geology*, v. 36, p. 235–238, doi:10.1130/G243326A.1.
- Christ, N., A. Immenhauser, F. Amour, M. Mutti, S. M. Agar, R. Always, and L. Kabiri, 2012, Characterization and interpretation of discontinuity surfaces in a Jurassic ramp setting (High Atlas, Morocco): *Sedimentology*, v. 59, p. 249–290, doi:10.1111/j.1365-3091.2011.01251.x.
- Coburn, T. C., J. M. Yarus, and R. L. Chambers, 2006, Geostatistics and stochastic modeling: Bridging into the 21st century, *in* T. C. Coburn, J. M. Yarus, and R. L. Chambers, eds., *Stochastic modeling and geostatistics: Principles, methods, and case studies, volume II: AAPG Computer Applications in Geology 5*, p. 3–9.
- Durlet, C., Y. Almeras, E. H. Chellai, S. Elmi, L. Le Callonnec,

- C. Lezin, and P. Neige, 2001, Anatomy of a Jurassic carbonate ramp: A continuous outcrop transect across the southern margin of the High Atlas (Morocco): *Géologie Méditerranéenne*, v. 28, p. 57–61.
- Eaton, T. T., 2006, On the importance of geological heterogeneity for flow simulation: *Sedimentary Geology*, v. 184, p. 187–201, doi:10.1016/j.sedgeo.2005.11.002.
- Ellouz, N., M. Patriat, J.-M. Gaulier, R. Bouatmani, and S. Sabounji, 2003, From rifting to Alpine inversion: Mesozoic and Cenozoic subsidence history of some Moroccan basins: *Sedimentary Geology*, v. 156, p. 185–212, doi:10.1016/S0037-0738(02)00288-9.
- Falivene, O., P. Arbués, J. Howell, J. A. Muñoz, O. Fernández, and N. Marzo, 2006, Hierarchical geocellular facies modeling of a turbidite reservoir analog from the Eocene of the Ainsa Basin, NE Spain: *Marine and Petroleum Geology*, v. 23, p. 679–701, doi:10.1016/j.marpetgeo.2006.05.004.
- Falivene, O., L. Cabrera, J. A. Muñoz, P. Arbués, O. Fernández, and A. Sáez, 2007, Statistical grid-based facies reconstruction and modeling for sedimentary bodies: Alluvial-palustrine and turbiditic examples: *Geologica Acta*, v. 5, p. 199–230.
- Gischler, E., and A. J. Lomando, 1999, Recent sedimentary facies of isolated carbonate platforms, Belize-Yucatan system, Central America: *Journal of Sedimentary Research*, v. 69, p. 747–763, doi:10.2110/jsr.69.747.
- Gradstein, F. M., J. G. Ogg, and A. G. Smith, 2004, *A geological time scale 2004*: Cambridge, United Kingdom, Cambridge University Press, 589 p.
- Gringarten, E., and C. V. Deutsch, 2001, Teacher's aide variogram interpretation and modeling: *Mathematical Geology*, v. 33, p. 507–534, doi:10.1023/A:1011093014141.
- Harris, P. M. M., 2010, Delineating and quantifying depositional facies patterns in carbonate reservoirs: Insight from modern analogs: *AAPG Bulletin*, v. 94, p. 61–86, doi:10.1306/07060909014.
- Immenhauser, A., 2009, Estimating paleo-water depth from the physical rock record: *Earth-Science Reviews*, v. 96, p. 107–139, doi:10.1016/j.earscirev.2009.06.003.
- Jacobshagen, V. H., R. Brede, M. Hauptmann, W. Heinitz, and R. Zylka, 1988, Structure and post-Paleozoic evolution of the central High Atlas, in V. H. Jacobshagen, ed., *The atlas system of Morocco: Studies on its geodynamic evolution*: Heidelberg, Germany, Springer-Verlag, p. 245–271.
- Jones, R. R., K. J. W. McCaffrey, J. Imber, R. Wightman, S. A. F. Smith, R. E. Holdsworth, P. Clegg, N. De Paola, D. Healy, and R. W. Wilson, 2008, Calibration and validation of reservoir models: The importance of high-resolution, quantitative outcrop analogs: *Geological Society (London) Special Publication* 309, p. 87–98.
- Jones, R. R., K. J. W. McCaffrey, P. Clegg, R. W. Wilson, N. S. Holliman, R. E. Holdsworth, J. Imber, and S. Waggott, 2009, Integration of regional to outcrop digital data: 3-D visualization of multiscale geological models: *Computers & Geosciences*, v. 35, p. 4–18, doi:10.1016/j.cageo.2007.09.007.
- Journel, A. G., R. Gunderso, E. Gringarten, and T. Yao, 1998, Stochastic modeling of a fluvial reservoir: A comparative review of algorithms: *Journal of Petroleum Science and Engineering*, v. 21, p. 95–121, doi:10.1016/S0920-4105(98)00044-8.
- Kenter, J., M. Harris, and A. Pierre, 2008, Digital outcrop models of carbonate platform and ramp systems: Analogs for reservoir characterization and modeling (abs.): AAPG International Conference and Exhibition, Cape Town, South Africa, October 26–29, 2008: <http://www.searchanddiscovery.com/documents/2008/08221kenter/> (accessed December 14, 2012).
- Kerans, C., F. J. Lucia, and R. W. Senger, 1994, Integrated characterization of carbonate ramp reservoir using Permian San Andres Formation outcrop analogs: *AAPG Bulletin*, v. 78, p. 181–216.
- Kjonesvik, D., J. Doyle, T. Jacobsen, and A. Jones, 1994, The effect of sedimentary heterogeneities on production from shallow marine reservoir: What really matters?: Society of Petroleum Engineers paper 28445, 14 p.
- Koehrer, B., B. S. C. Heymann, F. Prousa, and T. Aigner, 2010, Multiple-scale facies and reservoir quality variations within a dolomite body: Outcrop analog study from the Middle Triassic, SW German Basin: *Marine and Petroleum Geology*, v. 27, p. 386–411, doi:10.1016/j.marpetgeo.2009.09.009.
- Laville, E., A. Pique, M. Amrhar, and M. Charroud, 2004, A restatement of the Mesozoic Atlasic rifting (Morocco): *Journal of African Earth Science*, v. 38, p. 145–153, doi:10.1016/j.jafrearsci.2003.12.003.
- Lehrmann, D. J., and R. K. Goldhammer, 1999, Secular variation in parasequence and facies stacking patterns of platform carbonates: A guide to application of stacking patterns analysis in strata of diverse ages and settings, in P. M. Harris, A. H. Saller, and J. A. Simo, eds., *Advances in carbonate sequence stratigraphy: Applications to reservoirs, outcrop, and models*: Society for Sedimentary Geology Special Publication 63, p. 187–225.
- Manspeizer, W., J. H. Puffer, and H. L. Cousminer, 1978, Separation of Morocco and eastern North America: A Triassic–Liassic stratigraphic record: *Geological Society of America Bulletin*, v. 89, p. 901–920, doi:10.1130/0016-7606(1978)89<901:SOMAEN>2.0.CO;2.
- Mikes, D., and C. R. Geel, 2006, Standard facies models to incorporate all heterogeneity levels in a reservoir model: *Marine and Petroleum Geology*, v. 23, p. 943–959, doi:10.1016/j.marpetgeo.2005.06.007.
- Palermo, D., T. Aigner, N. Nardon, and W. Blendinger, 2010, Three-dimensional facies modeling of carbonate sand bodies: Outcrop analog study in an epicontinental basin (Triassic, southwest Germany): *AAPG Bulletin*, v. 94, p. 475–512, doi:10.1306/08180908168.
- Pierre, A., 2006, Un exemple de référence pour les systèmes de rampes oolitiques: Un affleurement continu de 37 km (falaise jurassiques d'Amellago, haut Atlas, Maroc): Ph.D. thesis, University of Bourgogne, France, 213 p.
- Pierre, A., C. Durllet, P. Razin, and E. H. Chellai, 2010, Spatial and temporal distribution of ooids along a Jurassic carbonate ramp: Amellago transect, High Atlas, Morocco: *Geological Society (London) Special Publication* 329, p. 65–88.
- Poisson, A., M. Hadri, A. Milhi, M. Julien, and J. Andrieux, 1998, The central High Atlas (Morocco): Litho- and

- chronostratigraphic correlations during Jurassic times between Tinjda and Tounfite: Origin of subsidence: *Mémoire du Museum d'Histoire Naturelle*, v. 179, p. 237–256.
- Pöppelreiter, M. C., M. A. Balzarini, B. Hansen, and R. Nelson, 2008, Realizing complex carbonate facies, diagenetic and fracture properties with standard reservoir modeling software: Geological Society (London) Special Publication 309, p. 39–49.
- Press, W. H., S. A. Teukolsky, W. T. Vetterling, and B. P. Flannery, 1992, *Numerical recipes in C: The art of scientific computing*: Cambridge, United Kingdom, Cambridge University Press, 994 p.
- Qi, L., T. R. Carr, and R. H. Goldstein, 2007, Geostatistical three-dimensional modeling of oolite shoals, St. Louis Limestone, southwest Kansas: *AAPG Bulletin*, v. 91, p. 69–96, doi:10.1306/08090605167.
- Rankey, E. C., 2004, On the interpretation of shallow shelf carbonate facies and habitats: How much does water depth matter?: *Journal of Sedimentary Research*, v. 74, p. 2–6, doi:10.1306/071803740002.
- Sech, R. P., M. D. Jackson, and G. J. Hampson, 2009, Three-dimensional modeling of a shelf-shelf parasequence reservoir analog: Part I. Surface-based modeling to capture high-resolution facies architecture: *AAPG Bulletin*, v. 93, p. 1155–1181, doi:10.1306/05110908144.
- Stanley, R. G., 1981, Middle Jurassic shoaling of the central High Atlas sea near Rich, Morocco: *Journal of Sedimentary Petrology*, v. 51, p. 895–907.
- Strasser, A., 1986, Ooids in Purbeck limestones (lowermost Cretaceous) of the Swiss and French Jura: *Sedimentology*, v. 33, p. 711–727, doi:10.1111/j.1365-3091.1986.tb01971.x.
- Strasser, A., and S. Védérine, 2009, Controls on facies mosaics of carbonate platforms: A case study from the Oxfordian of the Swiss Jura, in P. Swart, G. Eberli, J. McKenzie, I. Jarvis, and T. Stevens, eds., *Perspectives in carbonate geology*: International Association of Sedimentologists Special Publication, v. 41, p. 199–213.
- Strasser, A., B. Pittet, H. Hillgärtner, and J.-B. Pasquier, 1999, Depositional sequences in shallow carbonate-dominated sedimentary systems: Concepts for a high-resolution analysis: *Sedimentary Geology*, v. 128, p. 201–221, doi:10.1016/S0037-0738(99)00070-6.
- Studer, M., and R. Du Dresnay, 1980, Déformations sédimentaires en compression pendant le Lias supérieur et le Dogger, au Tizi n'Irhil (Haut Atlas central de Midelt, Maroc): *Bulletin de la Société Géologique de France*, v. 22, p. 391–397.
- Tomás, T., M. Zitzmann, M. Homann, M. Rumpf, F. Amour, M. Benisek, G. Marcano, M. Mutti, and C. Betzler, 2010, From ramp to platform: Building a 3-D model of depositional geometries and facies architectures in transitional carbonates in the Miocene, northern Sardinia: *Facies*, v. 56, p. 195–210.
- Verwer, K., G. Della Porta, O. Merino-tomé, and J. A. M. Kenter, 2009, Controls and predictability of carbonate facies architecture in a Lower Jurassic three-dimensional barrier-shoal complex (Djebel Bou Dahar, High Atlas, Morocco): *Sedimentology*, v. 56, p. 1801–1831.
- Warne, J. E., 1988, Jurassic carbonate facies of the central and eastern High Atlas rift, Morocco, in V. H. Jacobshagen, ed., *The atlas system of Morocco: Studies on its geodynamic evolution*: Heidelberg, Germany, Springer-Verlag, p. 169–199.
- Wilkinson, B. H., and C. N. Drummond, 2004, Facies mosaic across the Persian Gulf and around Antigua: Stochastic and deterministic products of shallow-water sediment accumulation: *Journal of Sedimentary Research*, v. 74, p. 513–526, doi:10.1306/123103740513.
- Wilkinson, B. H., C. N. Drummond, N. W. Diedrich, and E. D. Rothman, 1997, Biological mediation of stochastic peritidal carbonate accumulation: *Geology*, v. 25, p. 847–850, doi:10.1130/0091-7613(1997)025<0847:BMOSPC>2.3.CO;2.
- Wilkinson, B. H., C. N. Drummond, N. W. Diedrich, and E. D. Rothman, 1999, Poisson processes of carbonate accumulation on Paleozoic and Holocene platforms: *Journal of Sedimentary Research*, v. 69, p. 338–350, doi:10.2110/jsr.69.338.
- Willis, B. J., and C. D. White, 2000, Quantitative outcrop data for flow simulation: *Journal of Sedimentary Research*, v. 70, p. 788–802, doi:10.1306/2DC40938-0E47-11D7-8643000102C1865D.
- Wilmsen, M., and F. Neuweiler, 2008, Biosedimentology of the Early Jurassic postextinction carbonate depositional system, central High Atlas rift basin, Morocco: *Sedimentology*, v. 55, p. 773–807, doi:10.1111/j.1365-3091.2007.00921.x.
- Wright, V. P., and P. M. Burgess, 2005, The carbonate factory continuum, facies mosaics and microfacies: An appraisal of some of the key concepts underpinning carbonate sedimentology: *Facies*, v. 51, p. 17–23, doi:10.1007/s10347-005-0049-6.
- Zappa, G., R. Bersezio, F. Felletti, and M. Giudici, 2006, Modeling heterogeneity of gravel-sand, braided stream, alluvial aquifers at the facies scale: *Journal of Hydrology*, v. 325, p. 134–153, doi:10.1016/j.jhydrol.2005.10.016.
- Ziegler, P., 1994, Evolution of Peri-Tethyan basins as a mirror of Tethys dynamics, in F. Roure, ed., *Peri-Tethyan platforms*: Paris, France, Technip, p. 3–8.